CALIFORNIA INSTITUTE OF TECHNOLOGY

EARTHQUAKE ENGINEERING RESEARCH LABORATORY

ADDITIONAL INVESTIGATIONS ON A MATHEMATICAL MODEL FOR CALCULATION OF THE RUN-UP OF TSUNAMIS

BY

KENNETH LEON HEITNER

A REPORT ON RESEARCH CONDUCTED UNDER A GRANT FROM THE NATIONAL SCIENCE FOUNDATION

PASADENA, CALIFORNIA

JULY 1970

ADDITIONAL INVESTIGATIONS ON A MATHEMATICAL MODEL FOR CALCULATION OF THE RUN-UP OF TSUNAMIS

by

Kenneth Leon Heitner

California Institute of Technology
Pasadena, California

1970

ACKNOWLEDGMENT

The author wishes to thank Dr. George W. Housner for providing the opportunity to carry out this work and his guidance in the course of its execution. He also wishes to acknowledge the help of Drs. F. E. Marble, R. Raichlen, R. L. Street, and T. Y. Wu for some of the ideas and data in this work.

The work described in this report was supported by funding from the National Science Foundation.

INTRODUCTION AND ABSTRACT

Some of the concepts advanced in "A Mathematical Model for Calculation of the Run-Up of Tsunamis"[1] seemed to warrant further investigation. The motivation for this was a better understanding of the model and its usefulness, as well as the hope of being able to improve upon it. A summary of what was attempted and accomplished is presented below:

I. The bottom friction rule that the bottom shear stress was proportional to the velocity squared was investigated in more detail. It was found that the rule would be quite adequate, even though the run-up flow reversed itself and had large variations in depth near the leading edge.

II. Cnoidal-like waves were found to exist as solutions to the constrained flow equations. This was a natural generalization of the demonstration that the theory allowed for solitary waves.

III. More careful calculations were made for the shock solution utilizing the artificial viscosity term. The magnitude of the individual terms were calculated to get a better understanding of the nature of the solution. Several improvements to the artificial viscosity term were made in order to bring its behavior more into line with experimental data.

IV. Some run-up experiments were reproduced numerically to see how well the model could simulate reality. The results indicated the model was potentially useful.

[1] K. L. Heitner, "A Mathematical Model for Calculation of Run-up of Tsunamis," Earthquake Engineering Research Laboratory, California Institute of Technology, 1969.

TABLE OF CONTENTS

A NOTE ON BOTTOM FRICTION IN RUN-UP FLOWS

An important aspect of modelling tsunami run-ups is to correctly simulate the effects of bottom friction on the flow. Earlier models for run-up flows, (see Heitner (2)), used a steady flow bottom friction rule $\tau = Ku^2$. Here τ is the shear stress along the bottom, u the horizontal fluid velocity, and K a friction factor. Since friction is generally significant only on small slopes, the difference between u and the particle velocity tangential to the bottom is neglected.

Two natural problems evolve from the use of this rule. First, is that the run-up flow is non-steady and may undergo complete reversals of direction. This would affect the structure of the boundary layer and the resulting friction coefficient. Secondly, even for a steady flow, the coefficient K is a function of the ratio of the bottom roughness size to the flow depth. (It is assumed the flow will be rough turbulent). In the run-up flow the depth varies, particularly at the leading edge of the flow. The question is how well can a constant value of K represent the friction process in this case.

The first problem can be clarified by examining the nature of boundary layers in oscillating flows. Much experimental evidence in this area has been summarized by Jonsson (3). The experiments indicate that for a rough bottom, when the flow in the boundary layer is turbulent, the friction factor, K, is given by

$$K = \frac{0.0604}{\left(\log_{10}\left(\frac{22\delta}{r}\right)\right)^2} \qquad (1)$$

where r is the bottom roughness size and δ is the boundary layer thickness. When $2\delta = D$, where D is the total depth, (1) is the steady flow rough friction law.

Since the steady flow represents the greatest development of the boundary layer, i.e., a maximum value of $\delta = 2D$, it can be seen that an oscillating flow might tend to have a smaller δ, and consequently higher K.

The experiments indicate that δ is a function of a_m, the maximum particle amplitude in the direction of oscillation, and r, the bottom roughness size. This relationship is given by Jonsson as

$$30 \frac{\delta}{r} \log_{10}\left(30 \frac{\delta}{r}\right) = 1.2 \frac{a_m}{r} \tag{2}$$

Hence, if

$$1.2 \frac{a_m}{r} \geq \frac{15D}{r} \log\left(\frac{15D}{r}\right) \tag{3}$$

then the oscillations are sufficiently large so that the flow appears to be steady (locally) and the formula for a steady flow will be valid. If (3) is not satisfied, then $\delta < 2D$ and there will be an increase in K in accordance with (1).

In most cases, it will be seen that (3) is satisfied, i.e., the particle displacements are sufficiently large that a local steady flow condition is set up. Hence, the unsteadiness of the run-up flow does not invalidate the use of $\tau = Ku^2$.

The second problem, the variation of K with the local depth is especially puzzling for the run-up problem. Even when the friction is

set equal to zero, a run-up flow is a complicated function of several parameters. Adding a varying friction based on local depth can only make matters worse. A simplified problem that bears strong resemblance to the run-up problem is the classical dam break problem. Here a vertical dam at $x = 0$ is considered to impound water at constant depth for $-\infty < x < 0$. A dry level bed extends over $0 < x < +\infty$. At $t = 0$, the dam breaks and the flow begins. It is essentially an expansion wave with the depth going to zero at the leading edge. This is quite similar to the final phase of the run-up problem where a thin layer of water "shoots" up the beach.

For the dam-break problem, the solution without friction is known exactly and several approximate solutions using the bottom friction law $\tau = Ku^2$, with constant K, have been given by Dressler (1) and Whitham (3). Also experiments have been done on this problem by Dressler to examine the behavior with friction. Hence, it was felt that an understanding of the dam-break problem in the case where K is variable might contribute to an understanding of the effect of variable K in the run-up problem.

The approach used to solve the dam-break problem with a variable friction coefficient K is an extension of the method used by Whitham to solve the problem for K fixed. Consider Figure 1, showing the profile of the water free surface after the dam has broken. The profile with zero friction ($K = 0$) is given by

$$h^{\frac{1}{2}} = \frac{1}{3}\left(2 - \frac{x}{t}\right) \tag{4a}$$

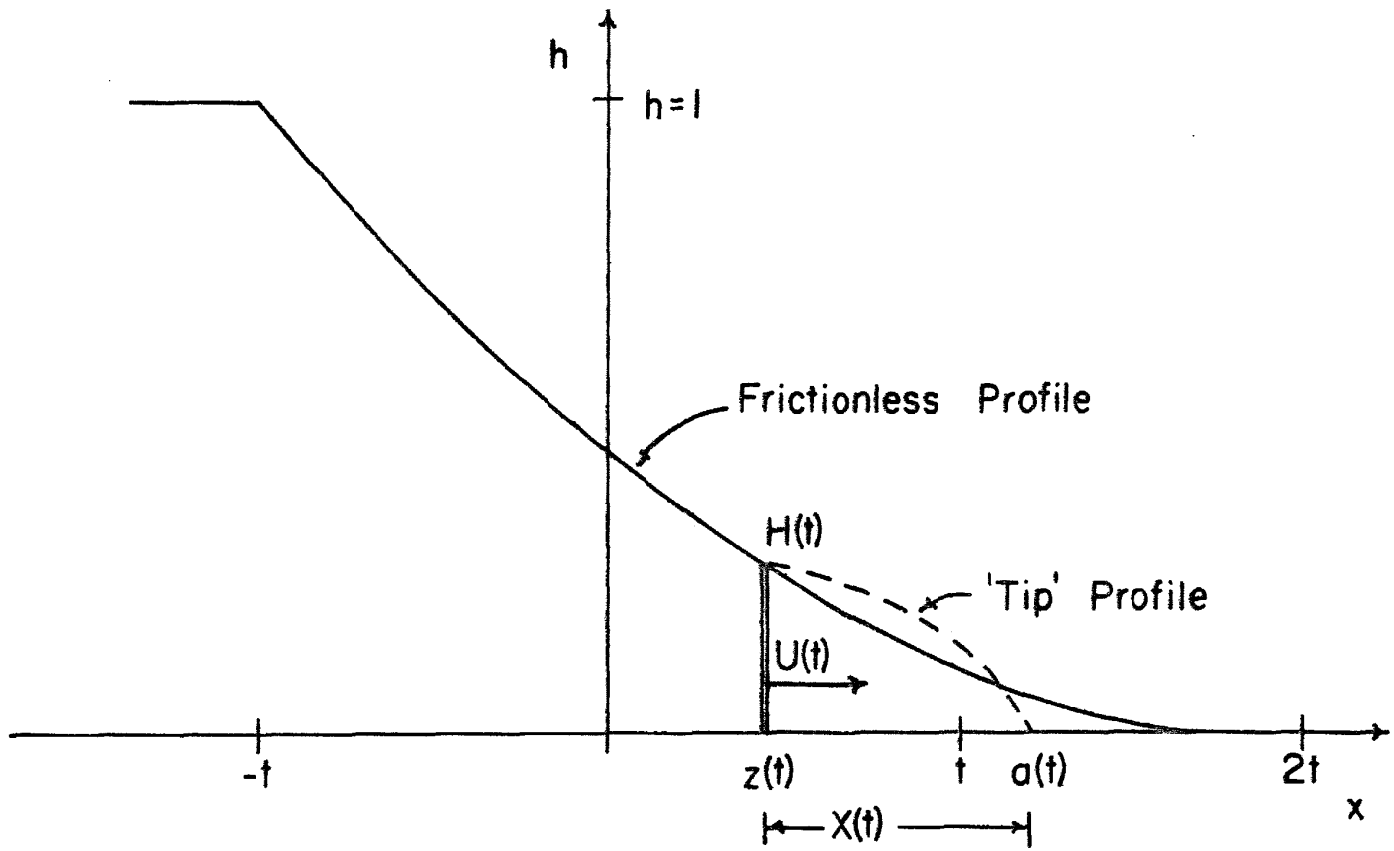

Figure 1 — Profile of dam-break problem.

where h is the depth, x is the horizontal coordinate, and t is the time after the dam breaks. (All constants, g for gravity, ρ for density, and h_o for initial depth are set equal to one for simplicity). The horizontal velocity u associated with this flow pattern is given by

$$u = \frac{2}{3}\left(\frac{x}{t} + 1\right) \tag{4b}$$

However, the presence of the bottom friction causes the fluid in the region $x \geq z(t)$ to pile up and form the tip region indicated by the broken line extending up to $x = a(t)$. Friction is only considered to act on the 'tip', that is for $z(t) \leq x \leq a(t)$. For $x \leq z(t)$ the flow is considered to be frictionless and given by (4a) and (4b).

Furthermore, it has been experimentally observed by Dressler that the 'tip' region moves almost as a rigid body. So an additional assumption used in the Whitham theory is that the 'tip' region behaves as a rigid body; that is, moves with the same velocity throughout.

If the horizontal velocity at $z(t)$, which is the same as that of the 'tip' region, is designated $U(t)$, and the depth at $z(t)$ is designated $H(t)$, then since (4a) and (4b) are valid, substitution yields

$$U = \frac{2}{3}\left(\frac{z}{t} + 1\right) \qquad H^{\frac{1}{2}} = \frac{1}{3}\left(2 - \frac{z}{t}\right) \tag{5a}$$

From this, the relations

$$z = \left(\frac{3}{2}U - 1\right)t \qquad H = \left(1 - \frac{1}{2}U\right)^2 \tag{5b}$$

$$U = 2\left(1 - H^{\frac{1}{2}}\right)$$

can be derived. If the volume of the tip for $z(t) \leq x \leq a(t)$ is designated

as M, it is found

$$M = \left(1 - \frac{U}{2}\right)^3 t = H^{3/2}\, t \tag{5c}$$

Since the tip is rigid, its momentum P is given by

$$P = MU \tag{6a}$$

When the rate of change of momentum of the tip region (dP/dt) is equated to the forces causing it, a momentum relation

$$M\frac{dU}{dt} = \frac{H^2}{2} - U^2 \int_{z(t)}^{a(t)} K(h)dx \tag{6b}$$

results.

In Whitham's solution for constant K, the integral in the last expression is merely $U^2 K(a - z)$, since K is constant. The only difficulty is in solving the ordinary differential equations for a(t). However for variable K, the problem is mathematically more complex.

In this case the desire is to study the growth of the tip region and to see what shape it takes. An additional parameter X, the length of the tip region is defined by

$$X(t) = a(t) - z(t) \tag{7}$$

The shape of the tip is given by a plot of H vs. X eliminating the parameter t (time) between them (see Figure 2).

By suitable manipulation, utilizing expressions (5), (6), and (7), coupled differential equations for H(t) and X(t) can be deduced. Since the integral in (6b) is eliminated by an additional differentiation, the system has second order derivatives of H(t). Defining $\frac{dH}{dt} = Q$, the final

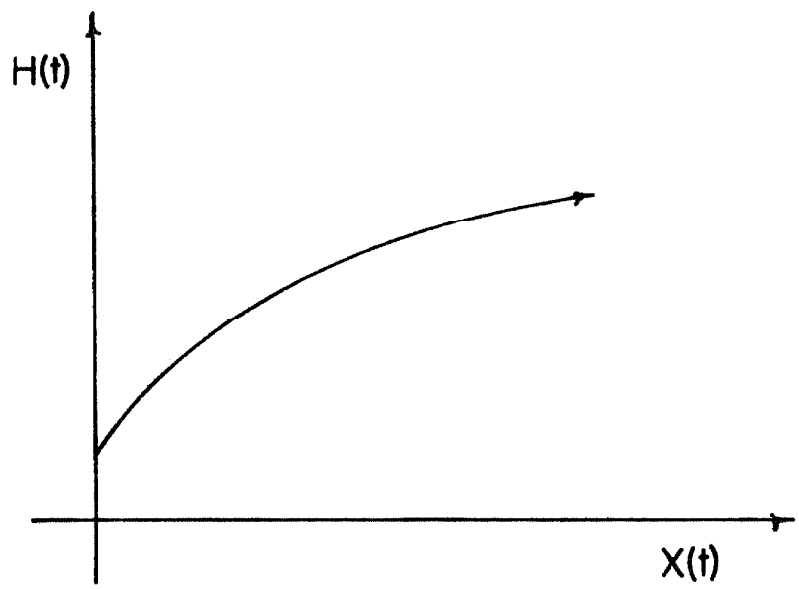

Figure 2 – Growth of tip region.

equations become

$$\frac{dX}{dt} = H^{\frac{1}{2}} \left(1 + \frac{3}{2}\frac{t}{H} Q\right)$$

$$\frac{dH}{dt} = Q$$

$$\frac{dQ}{dt} = -\frac{3}{2}\frac{Q}{t} - \left(Q + \frac{H}{2t}\right)\left(\frac{Q}{H(1-H^{\frac{1}{2}})}\right) \tag{8}$$

$$+ \frac{(1 - H^{\frac{1}{2}})^2}{Ht} \frac{.03}{\left(\log_{10}\left(\frac{11H}{r}\right)\right)^2} \frac{dX}{dt}$$

where the steady flow friction law

$$K \approx \frac{.06}{\left(\log_{10}\left(\frac{11H}{r}\right)\right)^2} \tag{9}$$

is used. The solution of (8) gives the shape of the tip region and indicates how rapidly it grows in time. In order to get the solution, the equations must be integrated from appropriate initial conditions. However, obvious initial conditions such as $H = 0$ and $X = 0$ at $t = 0$ will not work.

First of all, the equation is not really valid as the depth begins to approach the roughness size. Mathematically, this results in the log function in (8) "blowing" up when evaluated for $H \leq r/11$. Hence, the initial value for H should be at least equal to r. Since H will increase monotonically in time, it could be approximated by a series

$$H = a_o + a_1 t + a_2 t^2 + \ldots\ldots\ldots \quad (a_o \geq r/11) \tag{10}$$

for small time. The following expressions then result:

$$
\begin{aligned}
Q &= \frac{dH}{dt} = a_1 + 2a_2 t + \ldots \\
\frac{dQ}{dt} &= 2a_2 + 6a_3 t + \ldots \\
H^{\frac{1}{2}} &= \sqrt{a_o} + \frac{1}{2} \frac{a_1}{\sqrt{a_o}} t + \ldots
\end{aligned}
\tag{11}
$$

In addition, it is assumed that the solution for X can be written:

$$
\begin{aligned}
X &= b_o + b_1 t + b_2 t^2 + \ldots \\
\frac{dX}{dt} &= b_1 + 2b_2 t + \ldots
\end{aligned}
\tag{12}
$$

If these expressions are substituted in (8) and the coefficients of like powers of t are equated, it is found;

$$
a_1 = \frac{\left(1 - a_o^{\frac{1}{2}}\right)^2}{a_o^{\frac{1}{2}}\left(\frac{3}{2} + \frac{1}{1 - a_o^{\frac{1}{2}}}\right)} \frac{.03}{\left(\log_{10}\left(\frac{11 a_o}{r}\right)\right)^2} \tag{13}
$$

b_o is arbitrary. Thus, initial conditions for the problem are arrived at, i.e.,

$$
\begin{aligned}
H &= a_o + a_1 t \\
Q &= a_1 \\
X &= \text{arbitrary}
\end{aligned}
$$

(As an aid in writing the computer program to solve the equations set $a_o = r$ and $X = \sqrt{r}$.)

An additional problem is the fact that the equations are singular for $t = 0$ and the integration must start at a finite t. It was found

picking $t_o = r^2$ allowed solutions to be calculated without any numerical instability.

The integration was by a fifth order Runga-Kutta scheme using a time step equal to one-tenth the actual value of t. This gave very small time steps near the initial condition where high accuracy seemed needed to avoid erroneous solutions.

The solution was calculated until $H \geq 0.1$. The time to reach $H = 0.1$ is designated by $T_{0.1}$. If the solutions for various values of r are calculated, the results can be summarized in Figures 3 and 4. Figure 3 is plot of H vs. $X/T_{0.1}$. This curve is the same for all values of r, since the solutions are all "similar." Actually, there are slight differences near the initial point, but the general curve is the same.

Figure 4 summarizes the rate at which the tip region grows to $H = 0.1$. Additional solutions were run for constant values of K, by replacing the variable H in the friction expression by fixed values of $H = 0.1$ and $H = 0.01$. As can be seen, when the friction is a variable with depth, the tip growth times are about like that for $H = 0.065$. (This results from interpolating logarithmically between the curves for $H = 0.1$ and $H = 0.01$). However, 0.065 is about the average depth for the full tip region, and so the behavior is like that of constant K for a depth of 0.065.

In conclusion, it seems the effect of letting K vary with depth is not important, since the "tip" region moves as a rigid mass, and the

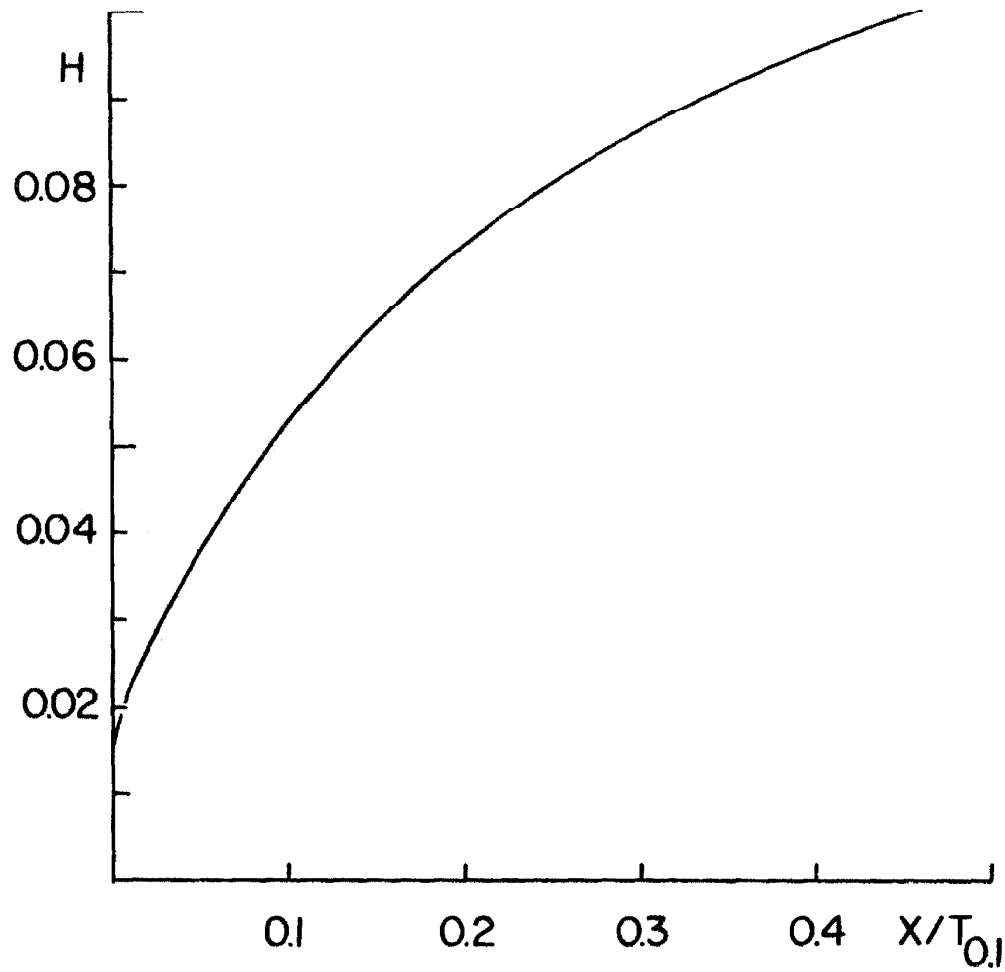

Figure 3 — Solution for tip shape.

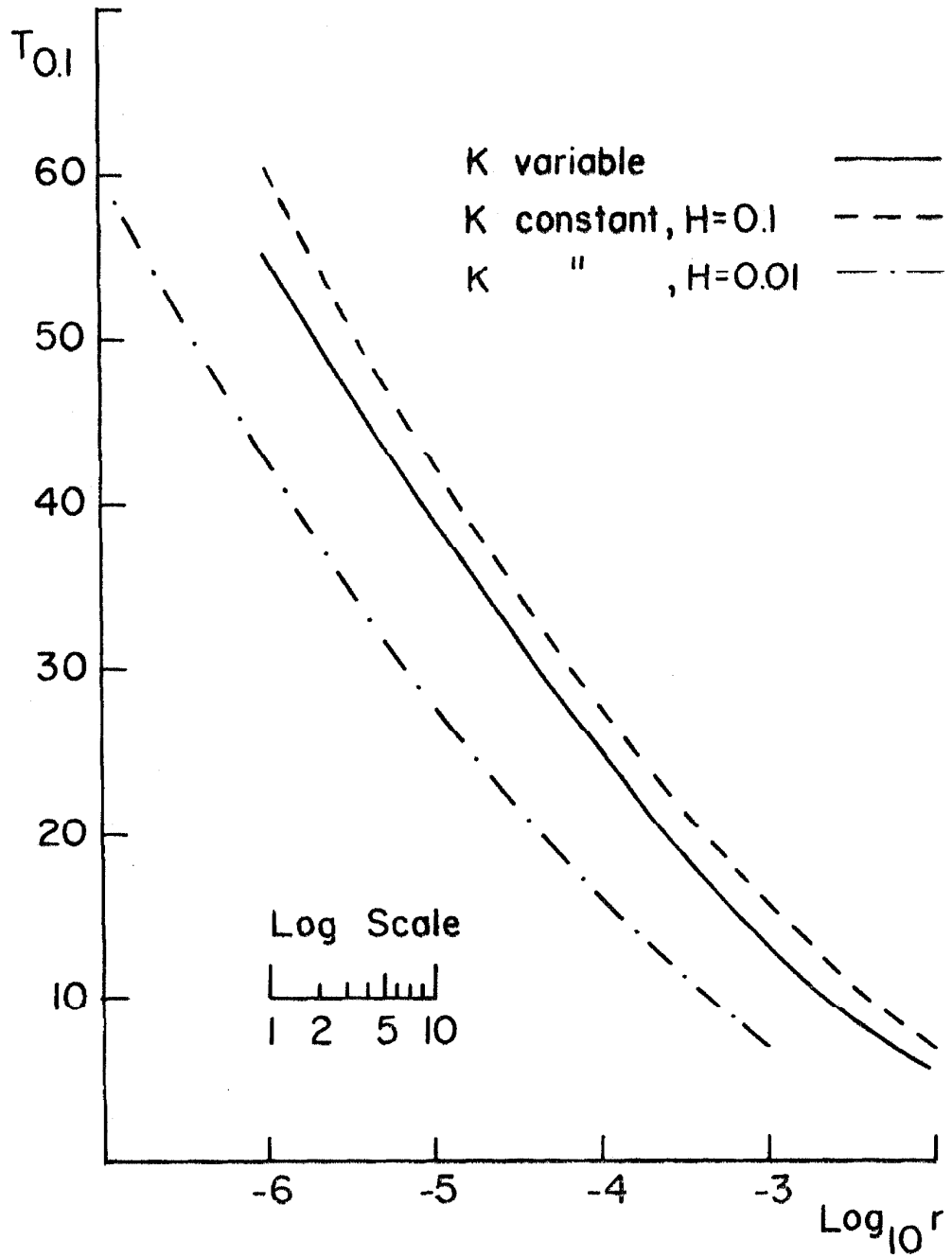

Figure 4 — Growth time of tip region vs. bottom roughness.

effect of a variable K is averaged out. If the correct K is chosen, the results will be consistent with the experimental behavior of the problem.

For the run-up problem, essentially the same behavior should take place, and the same reasoning apply. Near the front of the surge or rarefraction wave going up the beach, the motion is like a rigid mass of fluid and the friction coefficient is averaged out.

The finite element model for the run-up seems to be consistent with this type of behavior. The friction force for each element is averaged. Also the tip region, the element closest to the beach, moves as a rigid mass, without distortion.

Hence, the finite element model should give a fairly good modelling of the run-up process. What is needed are more careful checks against experimental results to give a better understanding of the capabilities and limitations of this method.

REFERENCES

(1) Dressler, R. F., Proc. X General Assembly, Int. Union of Geod. and Geophysics, Rome, 1954, Vol. 3, pp. 319-327.

(2) Heitner, K. L., "A Mathematical Model for Calculation of the Run-Up of Tsunamis," thesis presented to the California Institute of Technology, at Pasadena, California in 1969, in partial fulfillment of the requirements for the degree of Doctor of Philosophy.

(3) Johsson, I. G., "Wave Boundary Layers and Friction Factors," Proc. of the Tenth Conference on Coastal Engineering, ASCE, 1966, pp. 127-148.

(4) Whitham, G. B., "The Effect of Hydraulic Resistance in the Dam Break Problem," Proc. of Royal Soc. London, Series A, 227, pp. 399-407.

A NOTE ON CNOIDAL WAVES

The constrained flow theory, where the horizontal velocity is not a function of the depth, has been shown by Heitner (1) to exhibit a solution for a solitary-like wave of permanent form. This results from the inclusion of the kinetic energy of the vertical flow in the equations of motion. A natural question is to ask if this theory will also give rise to periodic waves of permanent form (and finite amplitude), similar to the cnoidal waves described in the theories of Korteweg and DeVries, and of Keulegan and Patterson (as summarized by Wiegel (2)).

The answer is that the existence of these waves can be demonstrated by examining the nature of the constrained flow equations. Integrals giving the profiles of the waves can be deduced from the equations and numerically evaluated to give the properties of these waves.

Consider the case where one examines a single wavelength of a permanent wave of finite amplitude in a reference frame moving at the wave velocity u_o. The wave, shown in Figure 1, appears as a steady flow with the symmetrical free surface profile. The maximum height of the wave with reference to the bottom is designated h_m. A wavelength (L) is defined as the distance between troughs.

The constrained flow equations are

$$h_t + (uh)_x = 0 \tag{1}$$

and

$$(uh)_t + \left(u^2h + \frac{1}{2}g\,h^2 + \frac{1}{3}h^3\,(u_x{}^2 - u_{xt} - uu_{xx})\right)_x = 0 \tag{2}$$

where u is the horizontal fluid velocity, h the height of the free surface above the bottom, x the horizontal coordinate, and t is time.

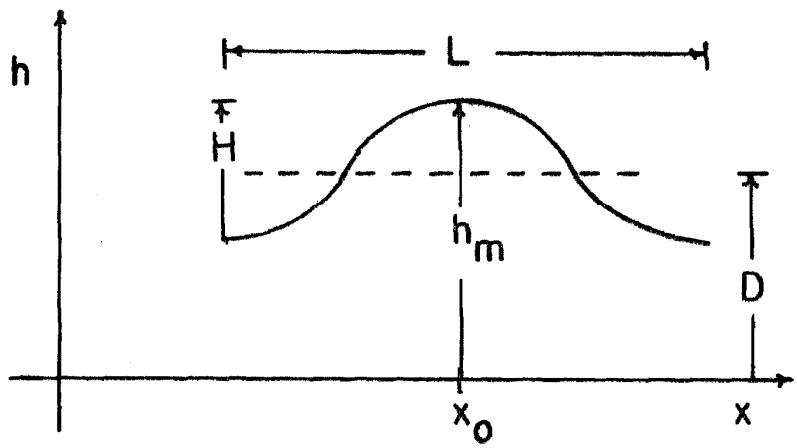

Figure 1 — Profile of permanent waveform

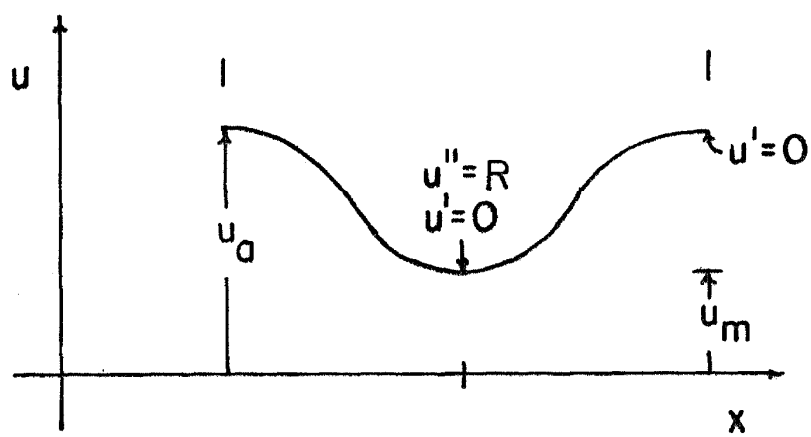

Figure 2 — Horizontal velocity profile for permanent waveform

For the steady flow involved here, the partial derivatives with respect to time vanish and the equations may be integrated once with respect to x to give

$$uh = A \tag{3}$$

$$u^2h + \frac{1}{2}gh^2 + \frac{1}{3}h^3\left((u')^2 - uu''\right) = B \tag{4}$$

where A and B are constants and

$$u' = \frac{du}{dx} \tag{5}$$

$$u'' = \frac{d^2u}{dx^2} \tag{6}$$

The constants, A and B, may be evaluated at the crest of the wave where $h = h_m$ and $u = u_m$. Using equation (3), the profile for u can be deduced as the inverse of that for h. This is shown in Figure 2. It is also necessary to let $u'' = R$, where $R > 0$ at $u = u_m$. Since this is a minimum point, $u' = 0$.

Hence, both A and B are evaluated

$$A = u_m h_m \tag{7}$$

$$B = u_m^2 h_m + \frac{1}{2} g h_m^2 - \frac{1}{3} h_m^3 u_m R \tag{8}$$

In order to integrate the equations (3) and (4) it is best to eliminate h between them and use

$$u'' = u' \frac{du'}{du} \tag{9}$$

to get

$$uA + \frac{gA^2}{2u^2} + \frac{A^3}{3u^2}\left((u')^2 - uu' \frac{du'}{du}\right) = B \tag{10}$$

This may be rearranged to give

$$d\left(\left(\frac{u'}{u}\right)^2\right) = \left(\frac{6u}{A^2} - \frac{6B}{A^3} - \frac{3g}{Au^2}\right) du \tag{11}$$

Integrating and using the additional condition that $u' = 0$ at $u = u_m$ gives

$$(u')^2 = \frac{3(u-u_m)\,u}{A^2}\left[u^2 + \left(u_m - \frac{2B}{A}\right)u + gh_m\right] \tag{12}$$

In order to obtain the profile indicated in Figure 2, u' must go to zero for $u = u_a$ at the wave trough. This means the quadratic portion of (12) (in brackets, [ ]), must contain at least one positive root at $u = u_a$, where $u_a > u_m$. *Since the product of the roots* (gh_m) *is always positive,* the second root of the quadratic (u_b) must also be positive. This root must be greater than u_a, so that the right-hand side of (12) is positive for $u_a \geq u \geq u_m$. This implies the sum of the roots $(2B/A - u_m) > 2u_a$.

For the roots to be real, an additional constraint is

$$(2B/A - u_m)^2 \geq 4gh_m \tag{13}$$

or

$$u_m + \frac{gh_m}{u_m} - 2\sqrt{gh_m} \geq \frac{2}{3} h_m^2 R \tag{14}$$

which places an upper limit on R (also $R > 0$).

Actually, since $u_b > u_a > u_m$, or

$$u_m + \frac{gh_m}{u_m} - \frac{2}{3} h_m^2 R \geq 2u_m$$

This gives

$$\frac{gh_m}{u_m} - u_m \geq \frac{2}{3} h_m^2 R > 0$$

which implies

$$u_m \leq \sqrt{gh_m} \tag{15}$$

In order to "construct" solutions for the "cnoidal-like" waves, a value of u_m is picked satisfying (15). Then a value of R satisfying (14) is selected. The roots of the quadratic may thus be calculated.

$$u_a, u_b = \frac{\left(\frac{2B}{A} - u_m\right) \pm \sqrt{\left(\frac{2B}{A} - u_m\right)^2 - 4gh_m}}{2} \tag{16}$$

In general, the waves are then represented by the equation

$$(u')^2 = \frac{3(u - u_m)u}{A^2} (u - u_a)(u - u_b) \tag{17}$$

where $u_a \geq u \geq u_m$.

The velocity profile of the wave, $u(x)$, may be calculated

$$\int_{u_m}^{u(x)} \frac{du}{\sqrt{3u(u - u_m)(u - u_a)(u - u_b)}} = \int_{x_o}^{x} \frac{dx}{A} \tag{18}$$

Also

$$\int_{u_m}^{u_a} = \int_{x_o}^{x_o + L/2} = \frac{L}{2A} \tag{19}$$

allowing the wavelength L to be obtained.

This integral can be evaluated numerically using Simpson's rule. Since the integrand in (18) is singular at the end points of the interval, it should be noted that integration by parts can remove this difficulty, since the integral is finite. Typically at $u = u_m$

$$\int_{u_m}^{u} \frac{du}{\sqrt{u - u_m}\,\sqrt{3u\,(u-u_a)(u-u_b)}} = \tag{20}$$

$$\frac{2\sqrt{u - u_m}}{\sqrt{3u(u-u_a)(u-u_b)}}\Bigg/_{u_m}^{u} + 3\int_{u_m}^{u} \frac{\sqrt{u-u_m}\; d[u(u-u_a)(u-u_b)]}{\left(3u\,(u-u_a)(u-u_b)\right)^{3/2}}$$

The wave speed u_o can be arrived at in two ways. First, u_o can be considered as simply the average velocity of the fluid, that is

$$u_o = \frac{1}{L}\int_0^L u\,dx \tag{21}$$

A second definition is arrived at by saying the net momentum in the fluid over a wavelength is zero, that is,

$$\int_0^L (u-u_o)\,h\,dx = 0 \tag{22}$$

Since

$$h = \frac{h_m u_m}{u}$$

$$\int_0^L u_m h_m\,dx = \int_0^L \frac{u_o u_m h_m}{u}\,dx$$

$$L = u_o \int_0^L \frac{dx}{u}$$

or

$$u_o = \frac{L}{\int_0^L \frac{dx}{u}} \tag{23}$$

The height of the wave, from crest to trough H, can be deduced from

$$H = h_m - \frac{u_m h_m}{u_a} \tag{24}$$

The still water depth D is given by

$$D = \frac{u_m h_m}{u_o} \tag{25}$$

From this information the parameters H/D, HL^2/D^3, and $u_o/\sqrt{gD}$ can be calculated. Note that D depends on the value of u_o, so that for each "solution," two slightly different sets of parameters are calculated.

Several typical solution values were calculated by an arbitrary procedure of first selecting a value of u_m such that

$$u_m \leq \sqrt{gh_m}$$

Then a value of R must be selected satisfying (14). If the maximum value of R is used, then the roots of quadratic (16) are equal, and the solitary-like wave solution exists. If R is slightly less than this value, a "cnoidal-like" wave results.

Because a computer was used to evaluate the solutions, only 12-13 significant figures were available to calculate the maximum R and a value slightly less than the maximum R. That is, if R_{max} is the maximum value of R, the largest $R < R_{max}$ that the computer can

calculate with 12 figures is $R_{max}(1 - 10^{-12})$. This made it impossible to evaluate solutions for L^2H/D^3 greater than about 300.

The solutions obtained are summarized in Table I, where they are compared with the values of Korteweg and DeVries; and of Keulegan and Patterson, as summarized by Wiegel. In general, the solutions to the constrained flow equations, using the definition of u_o given by (21) seem to give good agreement with the solutions of Keulegan and Patterson, though the values diverge for larger H/D. The divergence probably results from the inadequacy of the constrained flow in representing the horizontal velocity distribution at the larger H/D's.

Thus, it is seen that the constrained flow equations can approximate "cnoidal wave" behavior and the basic nature of the solution is related to solitary waves in at least one limiting case. The connection with sinusoidal wave solutions is less clear. Probably, a suitable analysis of the integral on the left-hand side of (18) is required. If this integral can be expressed in terms of elliptic functions, the theory could be used to give account of solutions ranging from solitary waves to sinusoidal waves. This would be similar to the more familiar cnoidal wave theories.

TABLE I

H/D (1)	HL^2/D^3 (2)	$u_o/\sqrt{gD}$ (3)	$u_o/\sqrt{gD}$ (4)	$u_o/\sqrt{gD}$ (5)	$u_o/\sqrt{gD}$ (6)
.162	236	1.041		1.05	1.04
.162	235		1.038	1.05	1.04
.160	118	1.027		1.04	1.03
.160	117		1.023	1.04	1.03
.343	262	1.087		1.12	1.09
.340	256		1.074	1.12	1.09
.336	127	1.057		1.09	1.06
.333	123		1.042	1.09	1.06
.546	290	1.135		1.20	1.15
.536	275		1.105	1.19	1.145
.530	137	1.089		1.15	1.105
.519	128		1.054	1.15	1.100
.775	323	1.188		1.28	1.21
.750	293		1.131	1.27	1.20
.746	148	1.123		1.23	1.155
.717	132		1.059	1.21	1.135

Note: Column (3) is based on u_o from Equation (21).

Column (4) is based on u_o from Equation (22).

Column (5) are the Korteweg and DeVries results.

Column (6) are the Keulegan and Patterson results.

References

(1) Heitner, K. L., "A Mathematical Model for Calculation of the Run-up of Tsunamis," thesis presented to the California Institute of Technology at Pasadena, California in 1969 in partial fulfillment of the requirements for the degree of Doctor of Philosophy.

(2) Wiegel, R. L., "A Presentation of Cnoidal Wave Theory for Practical Application," J. of Fluid Mechanics, Vol. 7, Part 2, 1960, pp. 273-86.

NOTES ON THE FORMATION OF SHOCKS IN RUN-UP FLOWS UTILIZING AN ARTIFICIAL VISCOSITY TERM

Introduction

In developing a model for run-up flows, Heitner (2) used an artificial viscosity term to allow for the formation of stable shocks when the waves broke. The term was an adoption of the artificial viscosity terms first used by Von Neumann and Richtmyer (4) to solve problems in gas dynamics. It allows the energy dissipation which takes place in the shock to be represented in the equations of motion, so that the shocks form automatically as part of the solution without any additional shock conditions. Examples were given of solutions for steady shocks and their use in the study of bore run-ups. Shocks were also allowed to form in the run-up solutions of other waveforms.

However, it was not clear from this first study that the term selected was the "best" artificial viscosity term in that it would give the best representation of the solutions with shocks. It also might lead to damping out of waveforms where no damping could be realistically expected (by dissipating energy in the wrong places).

In addition, the form of the artificial viscosity term raises a question because it resembles part of the term used to represent the kinetic energy of the vertical flow. Considering the constrained flow, where the horizontal velocity is constant with respect to the depth, the horizontal momentum equation is given by

$$(uh)_t + (u^2 h + \tfrac{1}{2} gh^2 + \tfrac{1}{3} \underbrace{h^3 (u_x{}^2}_{A} - u_{xt} - uu_{xx}) + \underbrace{\ell^2 h (u_x)^2}_{B} \text{Hysd}(-u_x))_x = 0 \tag{1}$$

where the original artificial viscosity term from reference (2) is included. Here u is the horizontal velocity, h the water depth, x is the horizontal coordinate, and t is time. Hysd(x) is defined as

$$\mathrm{Hysd}(x) = \begin{Bmatrix} 0 & x \leq 0 \\ 1 & x > 0 \end{Bmatrix}$$

The equation is for a flat bottom.

The term marked A , which partially represents the kinetic energy of the vertical flow, and term B, the artificial viscosity, are very similar. It was suggested that perhaps term B was not needed at all. Hence, it was desirable to examine the complete solutions for steady shocks to see how the terms varied through the shock. Thus a better understanding of the artificial viscosity term would be gained.

Use of Dimensionless Coefficient

As a first step towards improving the term, it was decided to eliminate the characteristic length "ℓ" associated with the coefficient ℓ^2. It seemed desirable to have a dimensionless coefficient, allowing the term to be valid for shocks without regard to scale size (i.e., local depth of the fluid). The simplest way to do this is to eliminate the ℓ^2 by using the dimensionless parameter $a = \ell/h$ and writing $a^2 h^3$ for $\ell^2 h$. The resulting horizontal momentum equation is

$$\begin{aligned} &(uh)_t + (u^2 h + \tfrac{1}{2} gh^2 + \tfrac{1}{3} h^3 (u_x{}^2 - u_{xt} - uu_{xx}) \\ &\quad + a^2 h^3 (u_x)^2 \,\mathrm{Hysd}\,(-u_x)\,)_x = 0 \end{aligned} \tag{2}$$

The equation can now be put in dimensionless form so that the solution for a shock is only a function of the Foude number Fr of the shock and the artificial viscosity coefficient a. (See Appendix A)

Calculation of Shock Solutions

In order to calculate the shock solutions, the momentum equation (2) is solved with the continuity equation (3).

$$h_t + (uh)_x = 0 \tag{3}$$

If the coordinate frame is chosen to be that moving with the shock, the flow is steady and the partial derivatives with respect to time are zero.

The equations may then be integrated once with respect to x. The conditions upstream of the shock, $u = u_1$, $h = h_1$, and $u' = u'' = 0$, may be used to evaluate the constants of integration. For convenience, let $h_1 = 1$. The results are

$$uh = u_1 h_1 = u_1$$

$$u^2h + \tfrac{1}{2}gh^2 + \tfrac{1}{3}h^3((u')^2 - uu'') + a^2h^3(u')^2\,\mathrm{Hysd}(-u') =$$

$$u_1^2 h_1 + \tfrac{1}{2}gh_1 = u_1^2 + \tfrac{1}{2}g \tag{4}$$

A free surface (h) profile of a shock is shown in Figure 1(b). The integrated continuity equation (4) indicates that the horizontal velocity (u) profile is the inverse of the h profile, as shown in Figure 1(a).

To find the shock solutions, the variable h can be eliminated from the set of equations (4). If u and u' are defined as $u = u_a$ and $u' = u_b$, the equations can be written as

$$\frac{du_a}{dx} = u_b$$

$$\frac{du_b}{dx} = \frac{3u_a^3}{u_1^2} + \frac{3g}{2u_1} + \frac{(u_b)^2}{u_a} + a^2\,\frac{3(u_b)^2}{u_a}\,\mathrm{Hysd}(-u_b) - \frac{3u_a^2}{u_1^3}(u_1^2 + \tfrac{1}{2}g) \tag{5}$$

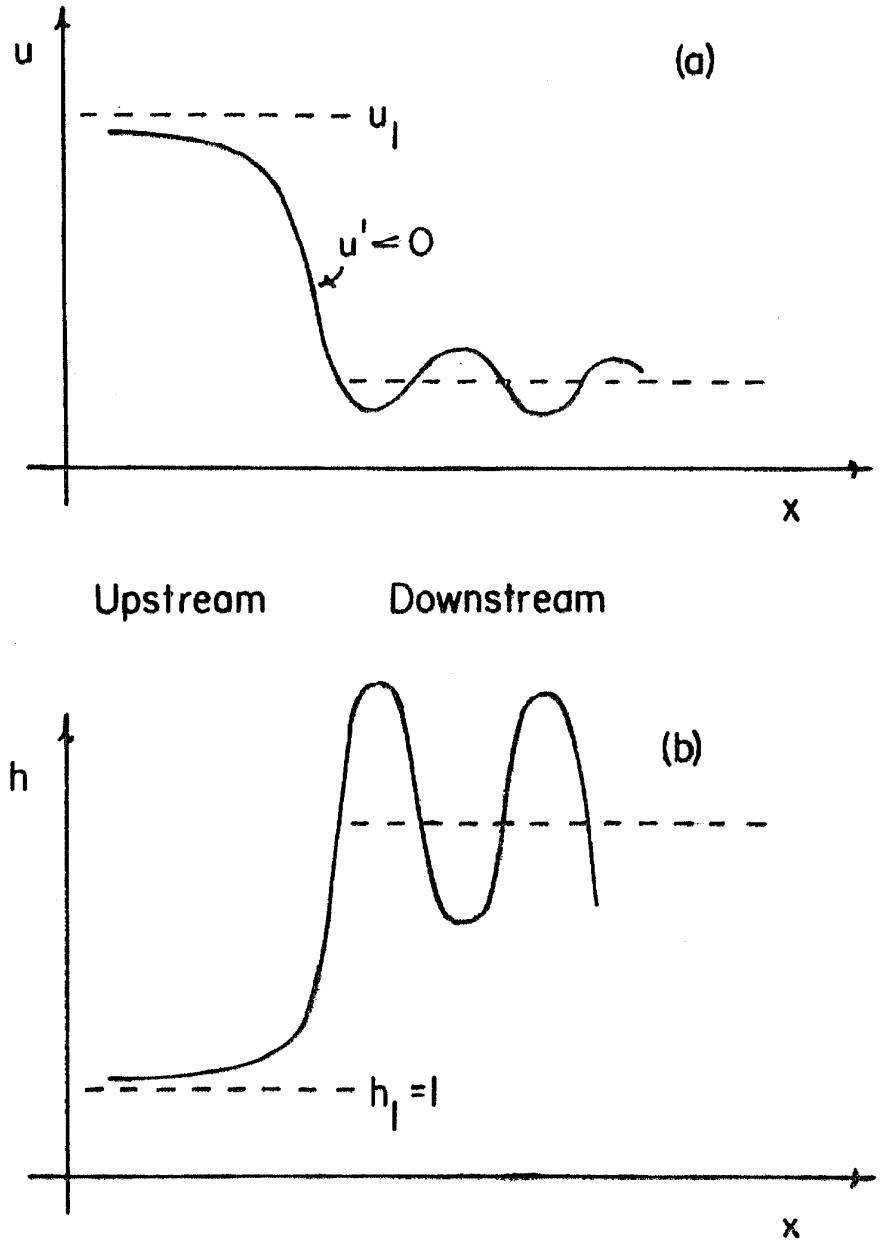

Figure 1 (a and b) -
Profile of a typical shock.

This system of first-order equations can be integrated numerically to give the shock profile. However, if one starts the integration at $u = u_1$, $u' = 0$, the equations are identically satisfied, and a constant solution results. It is necessary to derive the initial conditions from a perturbation calculation about the upstream conditions $u = u_1$, $u' = 0$.

This is done by using the relation $u'' = u' \frac{du'}{du}$ in equation (4). In addition, for the upstream side of the shock, $u' < 0$, so $\mathrm{Hysd}(u') = 1$. Equation (4) can be arranged so that the following results

$$\frac{d(u')^2}{du} + (u')^2 \left[-\frac{2}{u} - \frac{6a^2u}{u_1^2} \right] = \frac{6(u-u_1)}{u_1^2} \left[u^2 - \frac{gu}{2u_1} - \frac{g}{2} \right] \tag{6}$$

If the solution is assumed to be in the form

$$(u')^2 = A + B(u-u_1) + C(u-u_1)^2 + \ldots \tag{7}$$

for small values of $(u-u_1)$, the constants A, B, C .... can be determined. Since $u' = 0$ for $u = u_1$, $A = 0$. Expanding the bracketed expressions in (6) in terms of $(u-u_1)$ and substituting (7) yields the following

$$B = 0$$

$$C = 3(1 - g/u_1^2) = 3\left(1 - \frac{1}{Fr^2}\right) \tag{8}$$

where Fr is the Froude number of the shock.

Thus the perturbation expansion is

$$(u')^2 = 3\left(1 - \frac{1}{Fr^2}\right)(u-u_1) + O(u-u_1)^3$$

Neglecting the $O(u-u_1)^3$ and higher terms, the first approximation for the solution is then

$$(u') = \sqrt{3\left(1 - \frac{1}{Fr^2}\right)} \quad (u-u_1)$$

Integrating the equation

$$\int_{u_1}^{u} \frac{du}{u_1 - u} = -\sqrt{} \int_{-\infty}^{x} dx$$

where the downstream condition $u = u_1$ is satisfied at $x = -\infty$.

$$\ln (u_1 - u) - (-\infty) = \sqrt{} \left(x - (-\infty) \right)$$

The infinite terms cancel out. The quantity $- \ln (u_1)$ can be added to the left hand side to shift the origin and give

$$\ln \left(\frac{u_1 - u}{u_1} \right) = x\sqrt{}$$

$$\frac{u_1 - u}{u_1} = \exp (x \sqrt{})$$

$$u = u_1 \left(1 - \exp \left\{ x \sqrt{3 (1 - \frac{1}{Fr^2})} \right\} \right) \tag{9}$$

This solution can be used to arrive at initial conditions for the numerical integration. Typically, the initial conditions arrived at by using $x = -5$ were adequate, because of the stable nature of the shock solution (see Appendix B). After the solution $u(x)$ is calculated, the free surface profile of the shock $h(x)$ is obtained from the continuity relation.

Calculation of Momentum and Energy Terms

The shock solution can be used to evaluate the individual terms of momentum and energy equations as these quantities vary through the shock. This enables a greater understanding of the significance of each term.

Since the flow is steady, both equations are integrated once and the right hand side is evaluated with the upstream conditions. The horizontal momentum equation is then

$$\underbrace{u^2h}_{A} + \underbrace{\tfrac{1}{2}gh^2}_{B} + \underbrace{\tfrac{1}{3}h^3\left((u')^2 - uu''\right)}_{C}$$

$$\underbrace{+ u^2h^3(u')^2\,\mathrm{Hysd}(-u')}_{D} = u_1^2 + g/2 \tag{10}$$

Term A is the horizontal fluid momentum. Term B is the total horizontal force due to the hydrostatic pressure. Term C is the total horizontal force due to the pressures arising from the vertical fluid motion. Term D is the artificial viscosity force.

The energy equation is written as

$$\underbrace{\tfrac{1}{2}u^3h}_{A} + \underbrace{\tfrac{1}{2}gh^2u}_{B} + \underbrace{\tfrac{1}{6}u(u')^2h^3}_{C} + \underbrace{u\left(\tfrac{1}{2}gh^2 + \tfrac{1}{3}h^3\left((u')^2 - uu''\right)\right)}_{D}$$

$$\underbrace{+ \int u\left\{a^2h^3(u')^2\,\mathrm{Hysd}(-u')\right\}' dx}_{E} = \frac{u_1^3}{2} + u_1 g \tag{11}$$

Term A is the horizontal kinetic energy. Term B is the potential energy due to the gravity field. Term C is the vertical kinetic energy. Term D is the work done against the change in the hydrostatic pressure and the pressure due to vertical motion. Term E is the energy dissipated by the artificial viscosity term. A complete explanation of the energy equation is given in Appendix C.

Discussion of Shock Solutions

Figures 2, 3, and 4 give typical examples of computed shock solutions for Fr = 3.3 and different values of a^2. For the graphs of the momentum and energy terms, the lettered regions correspond to

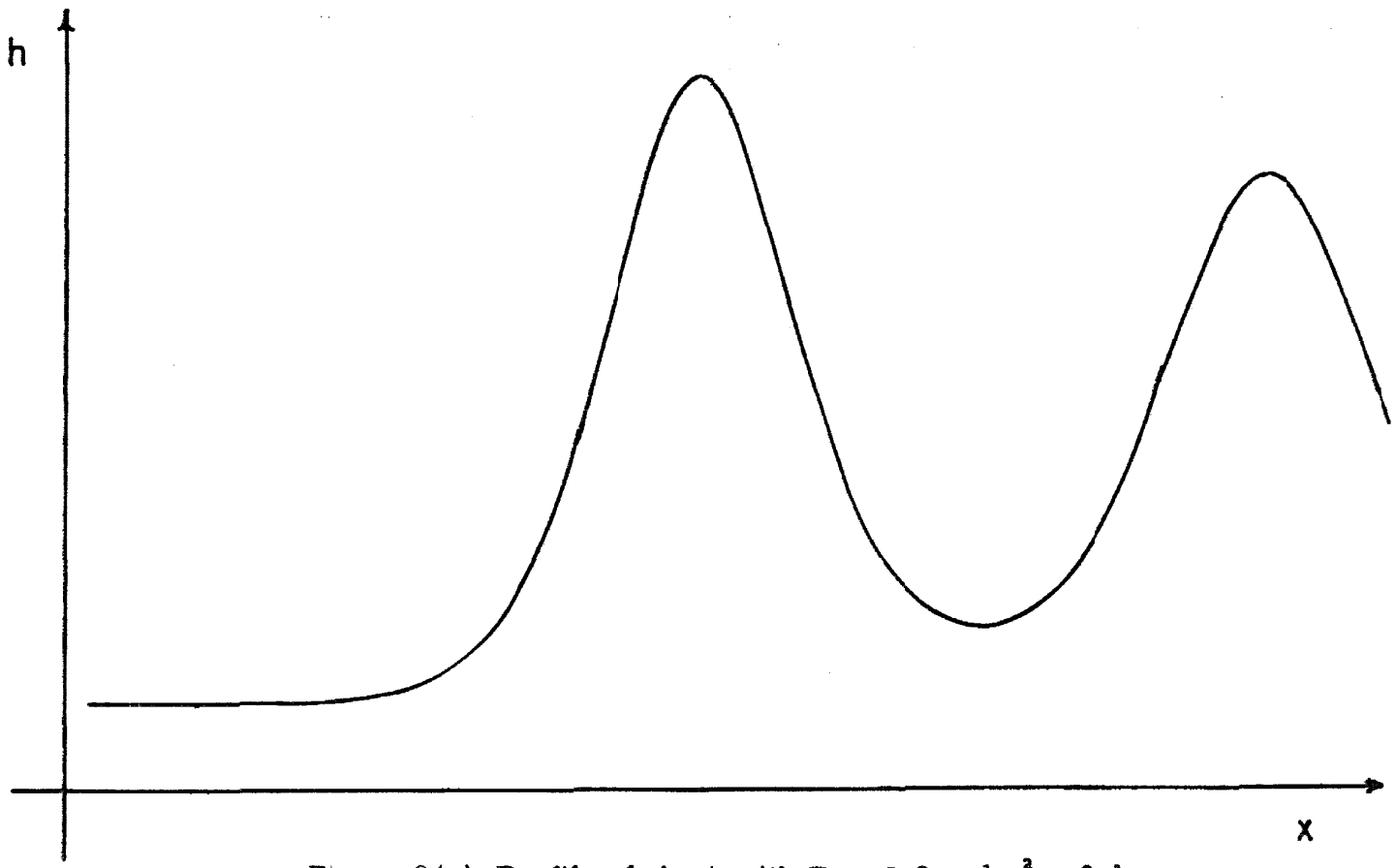

Figure 2(a) Profile of shock with Fr = 3.3 and a^2 = 0.1.

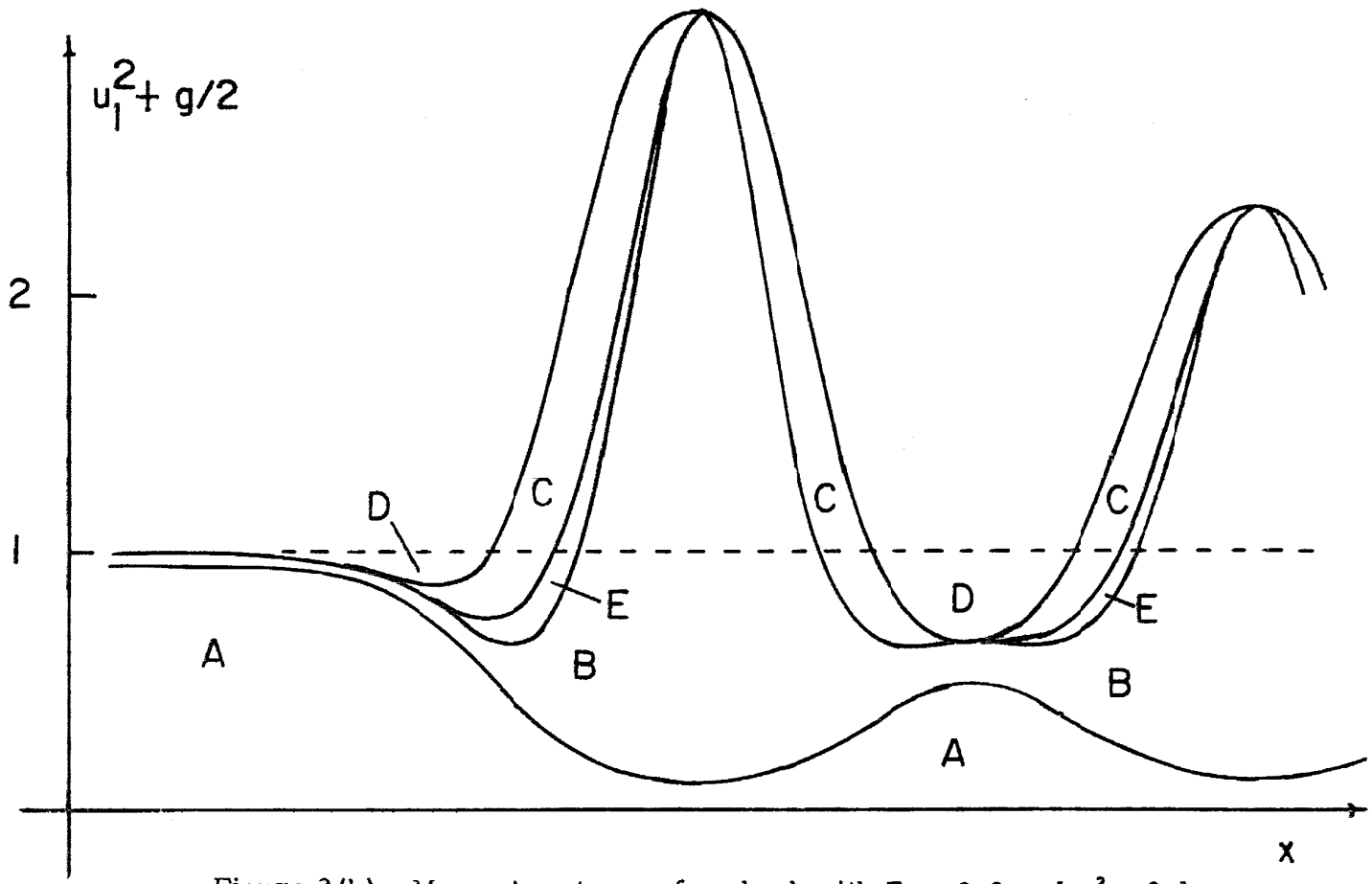

Figure 2(b) - Momentum terms for shock with $Fr = 3.3$ and $a^2 = 0.1$.

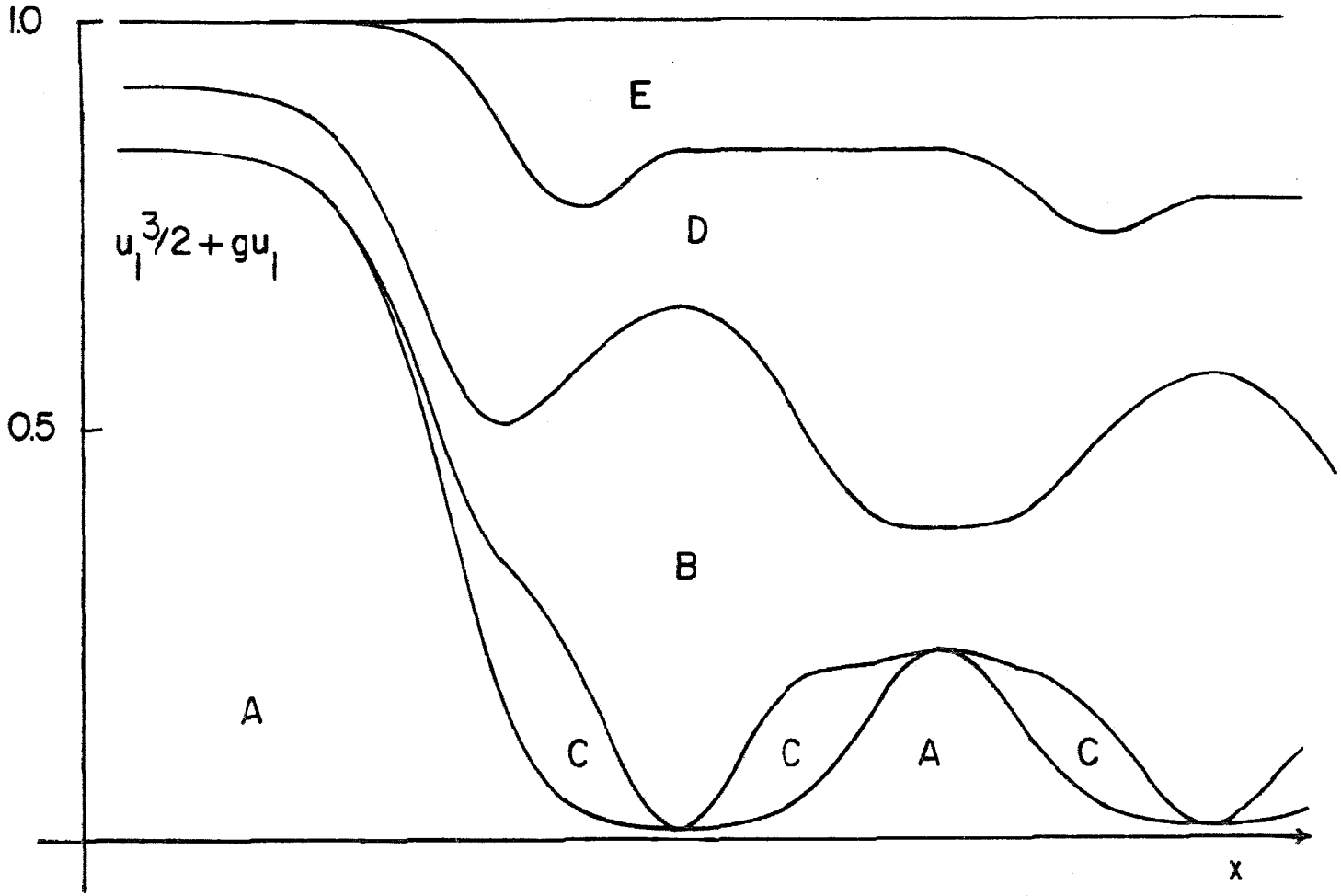

Figure 2(c) - Energy terms for shock with Fr = 3.3 and a^2 = 0.1.

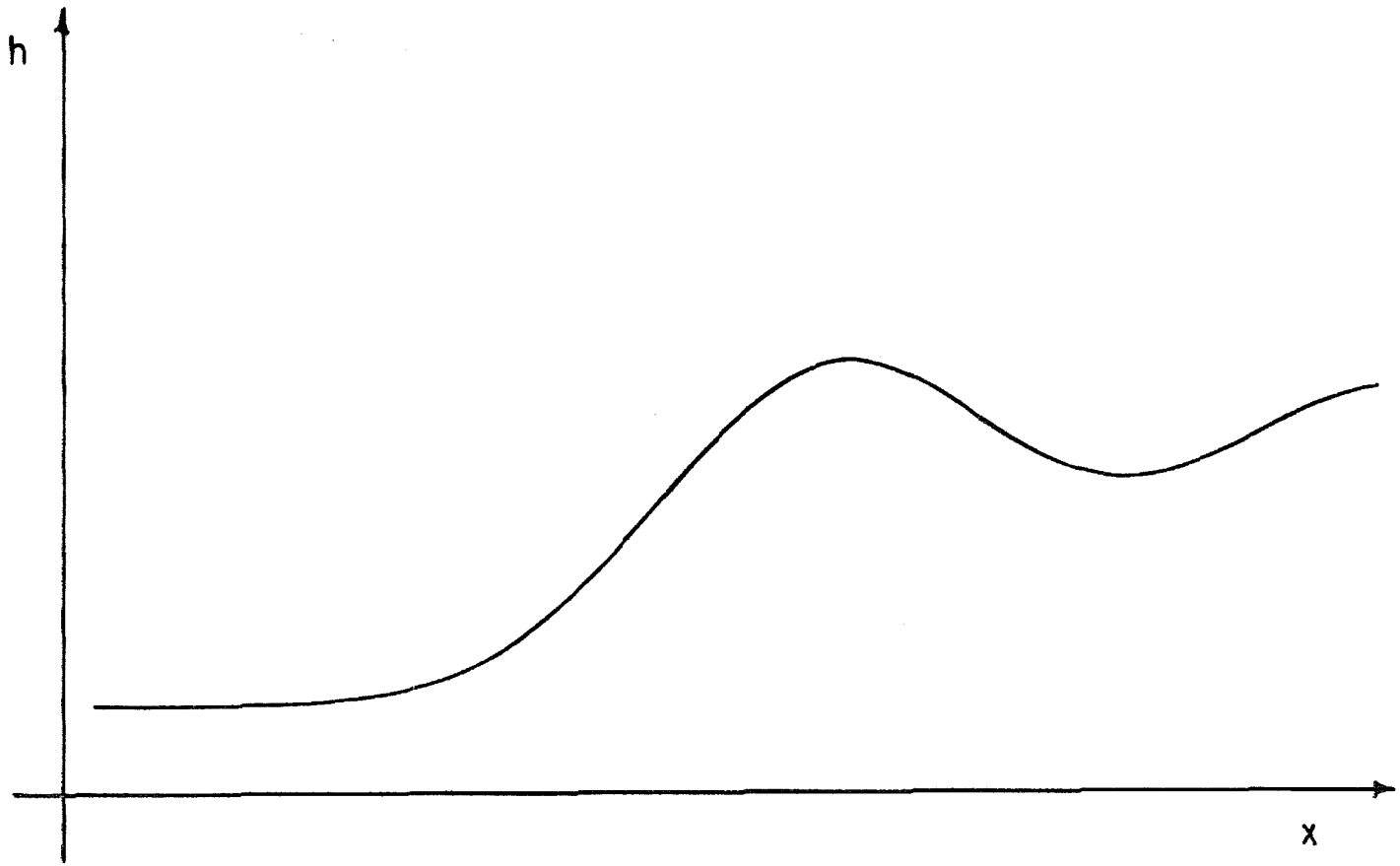

Figure 3 (a) - Profile of shock with Fr = 3.3 and a^2 = 1.0.

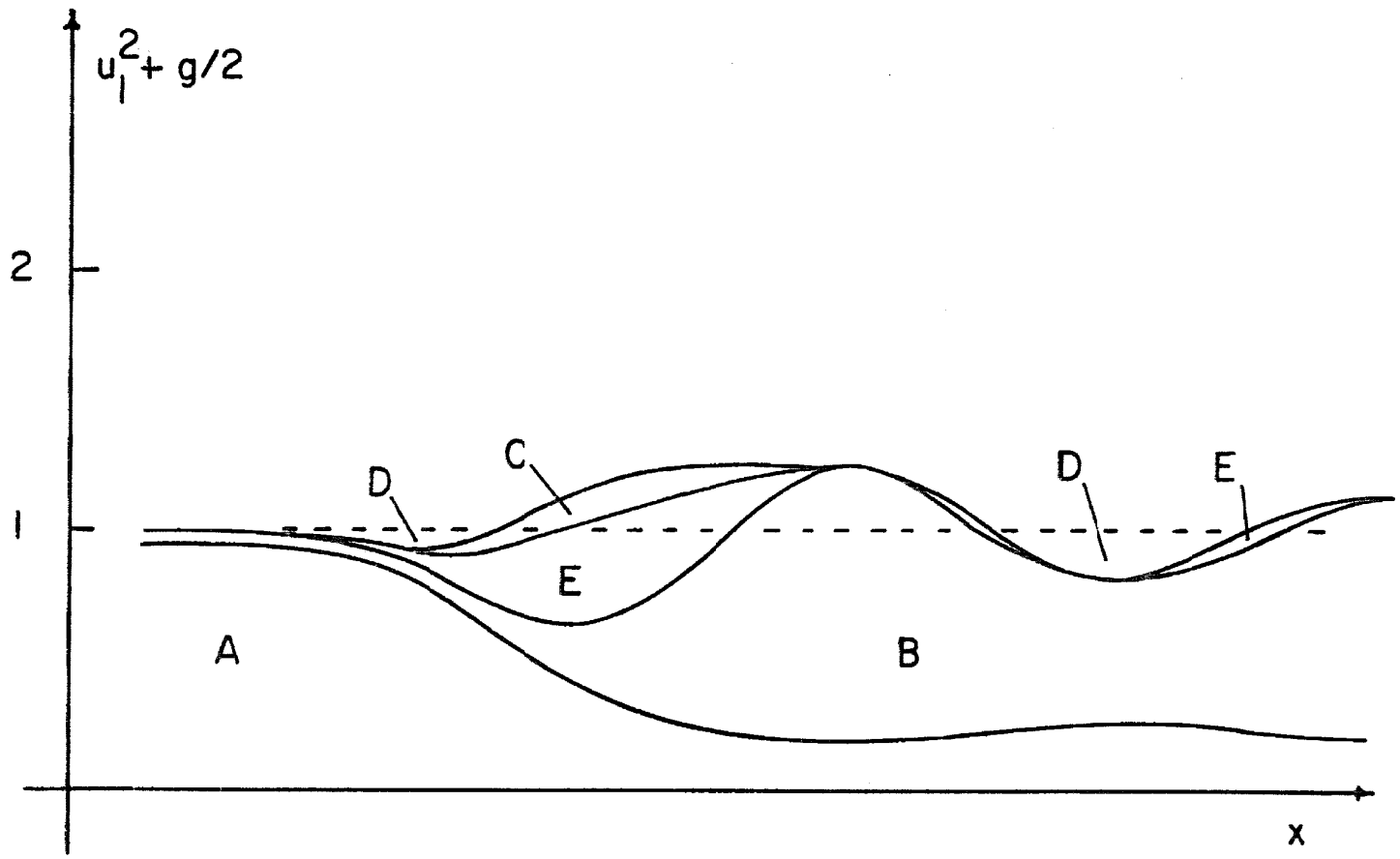

Figure 3 (b) - Momentum terms for shock with Fr = 3.3 and a^2 = 1.0.

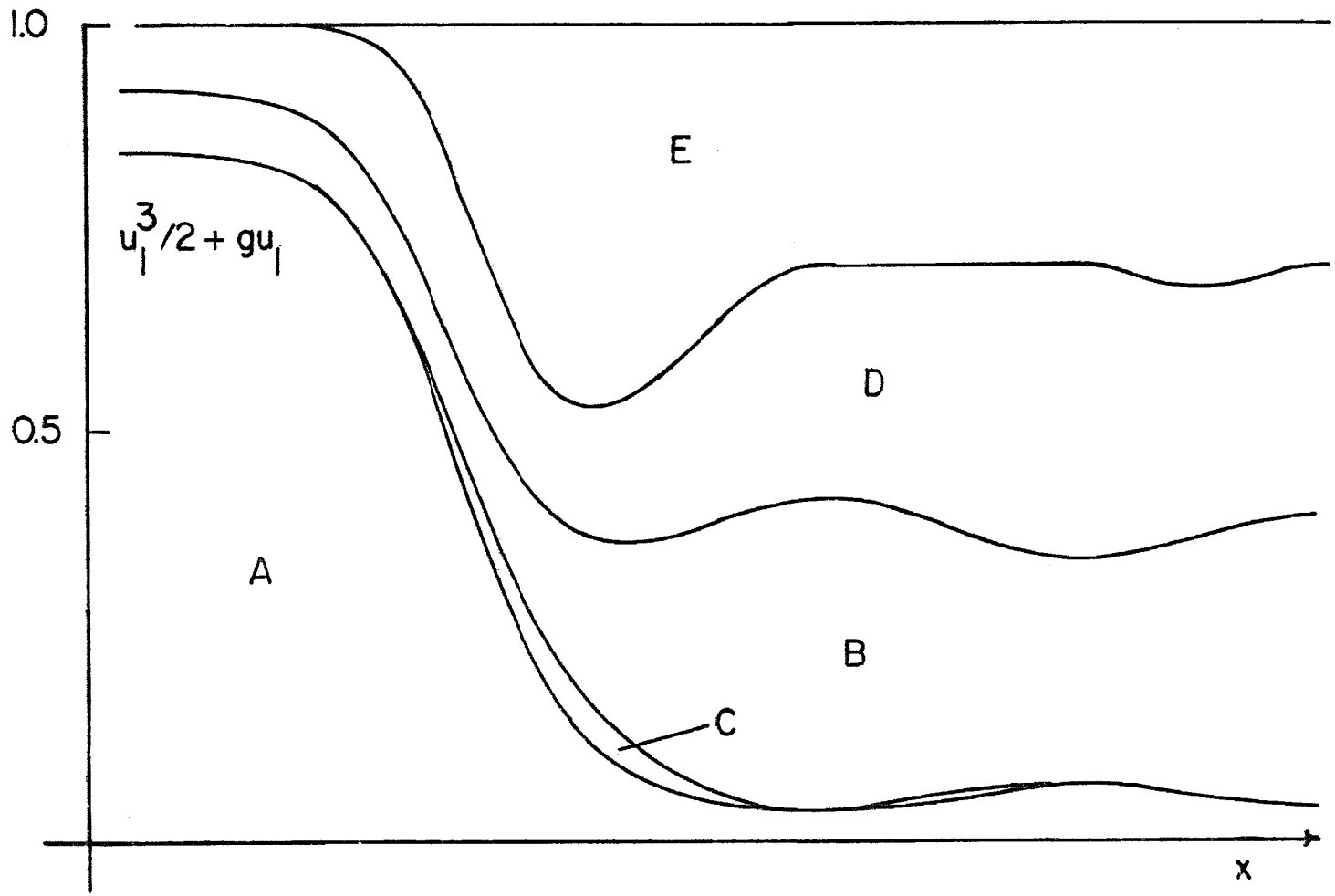

Figure 3(c) - Energy terms for shock with Fr = 3.3 and $a^2 = 1.0$.

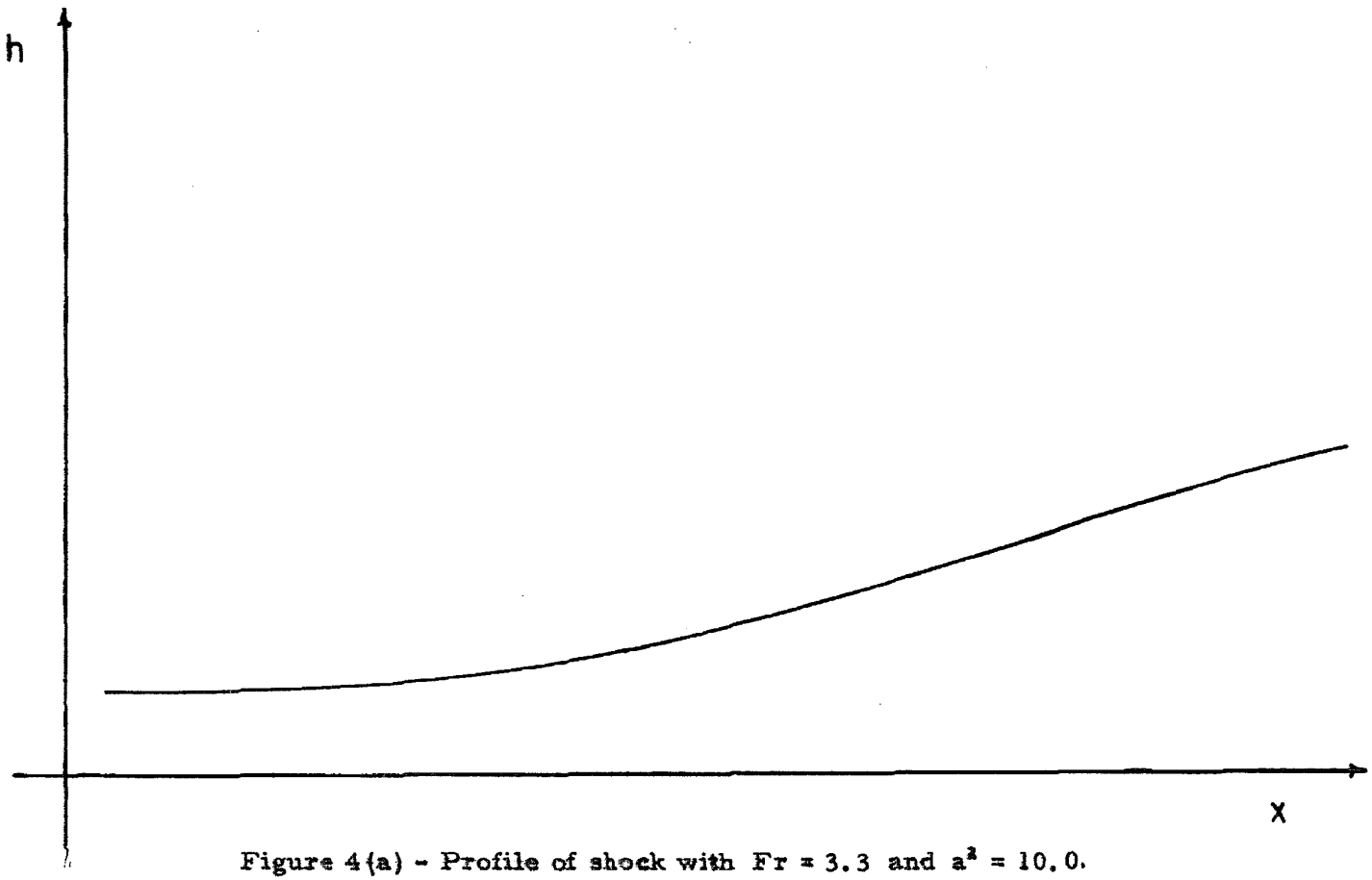

Figure 4(a) - Profile of shock with $Fr = 3.3$ and $a^2 = 10.0$.

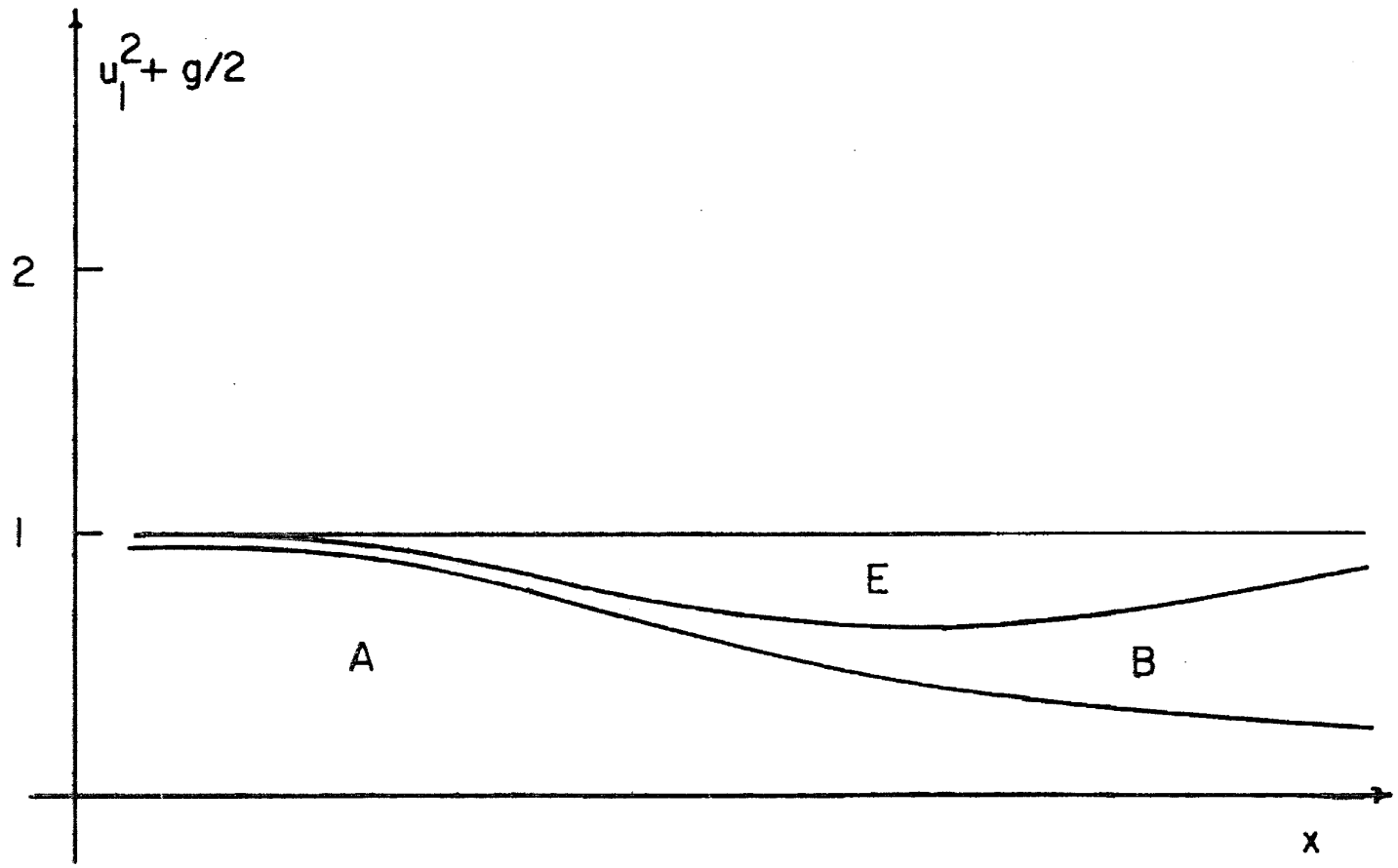

Figure 4(b) - Momentum terms for shock with $Fr = 3.3$ and $a^2 = 10.0$

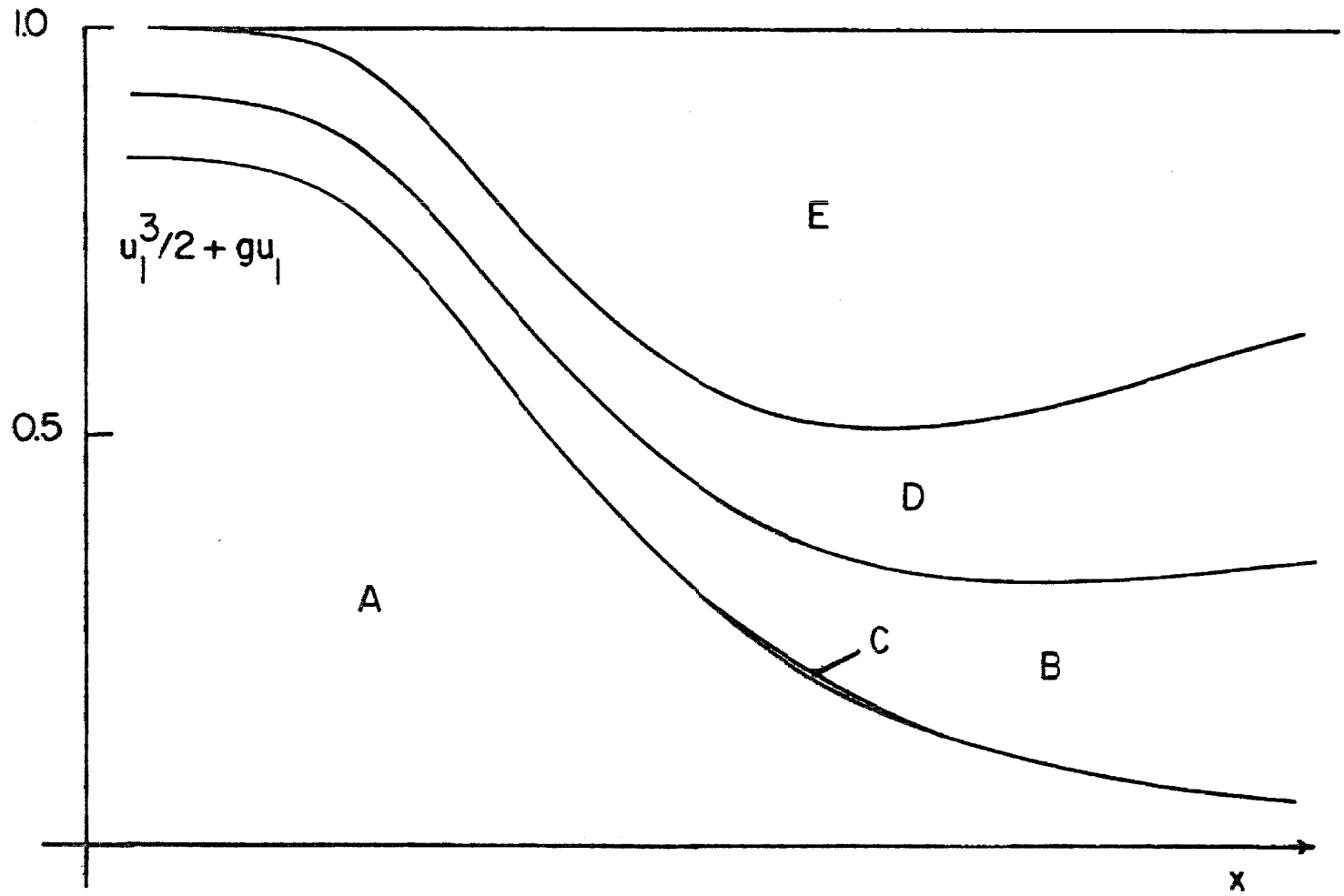

Figure 4(c) - Energy terms for shock with Fr = 3.3 and a^2 = 10.0.

values of the similarly lettered terms of equations (10) and (11) respectively. For $a^2 = 0.1$, Figure 2(a), the shock front is quite steep, but the shock is followed by large oscillations on the downstream side. They result from the fact that insufficient energy is dissipated by the artificial viscosity term, the difference going into the downstream oscillations. The oscillations damp out as the artificial viscosity term removes some energy on each cycle.

If the Froude number is held constant and a^2 is increased, the energy lost in the shock is closer to the equilibrium value for the shock, and the downstream oscillations are considerably smaller. This is seen in Figure 3(a) ($a^2 = 1.0$) and Figure 4(a) ($a^2 = 10.0$). The artificial viscosity term limits the maximum rate of change of u, "smearing" out the shock width. This is seen best by examining the magnitude of the terms in the momentum equation in Figure 4(b). Almost no force results from the gradual vertical motion of the fluid passing through the shock at $a^2 = 10.0$. The momentum equation is balanced entirely by the artificial viscosity term in the transition region.

On the other hand, if a^2 is held constant (at $a^2 = 1.0$) and Froude number is allowed to vary, the shock behavior tends to be independent of the Froude number. That is, the ratio between the size of the jump and the size of downstream undulations does not vary rapidly. This is seen in Figure 5(a) for Fr = 2.3 and Figure 6(a) for Fr = 5.7. Also, the maximum slope in the shock profiles is about the same for different values of Fr. Of course, for higher Froude numbers, a larger portion of the total energy is dissipated in the shock. See Figures 3(c), 5(c), and 6(c).

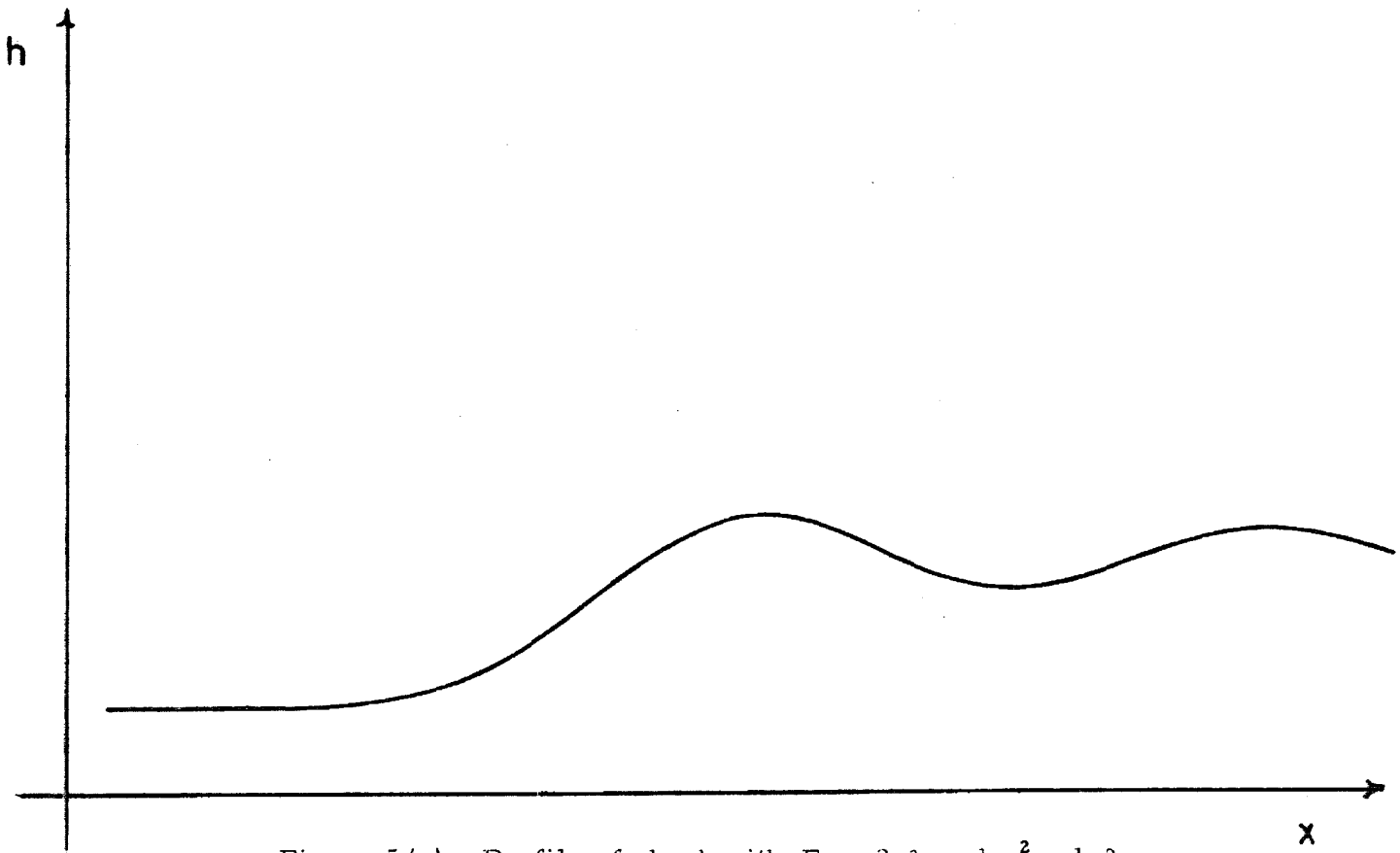

Figure 5 (a) - Profile of shock with Fr = 2.3 and a^2 = 1.0.

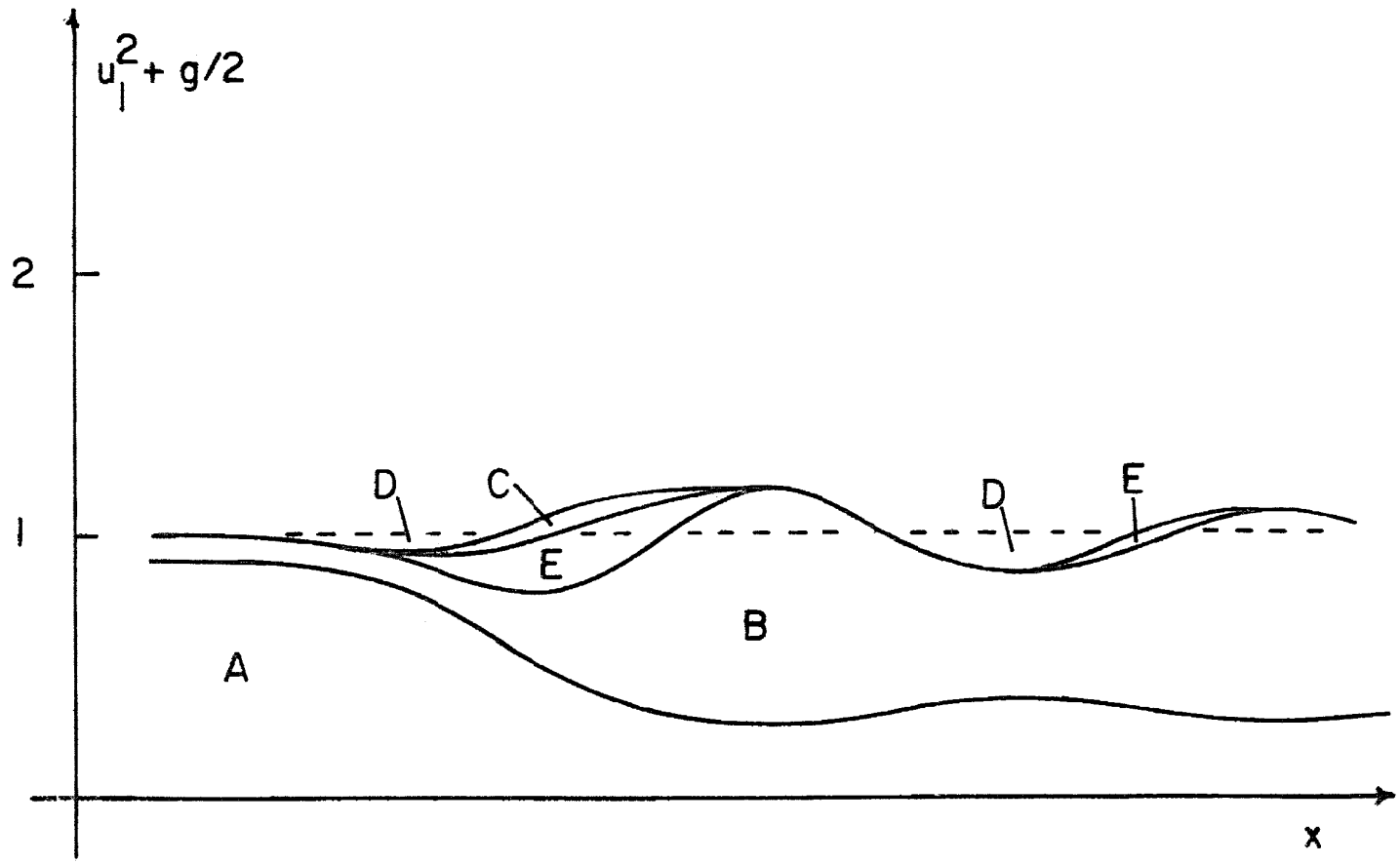

Figure 5(b) - Momentum terms for shock with $Fr = 2.3$ and $a^2 = 1.0$.

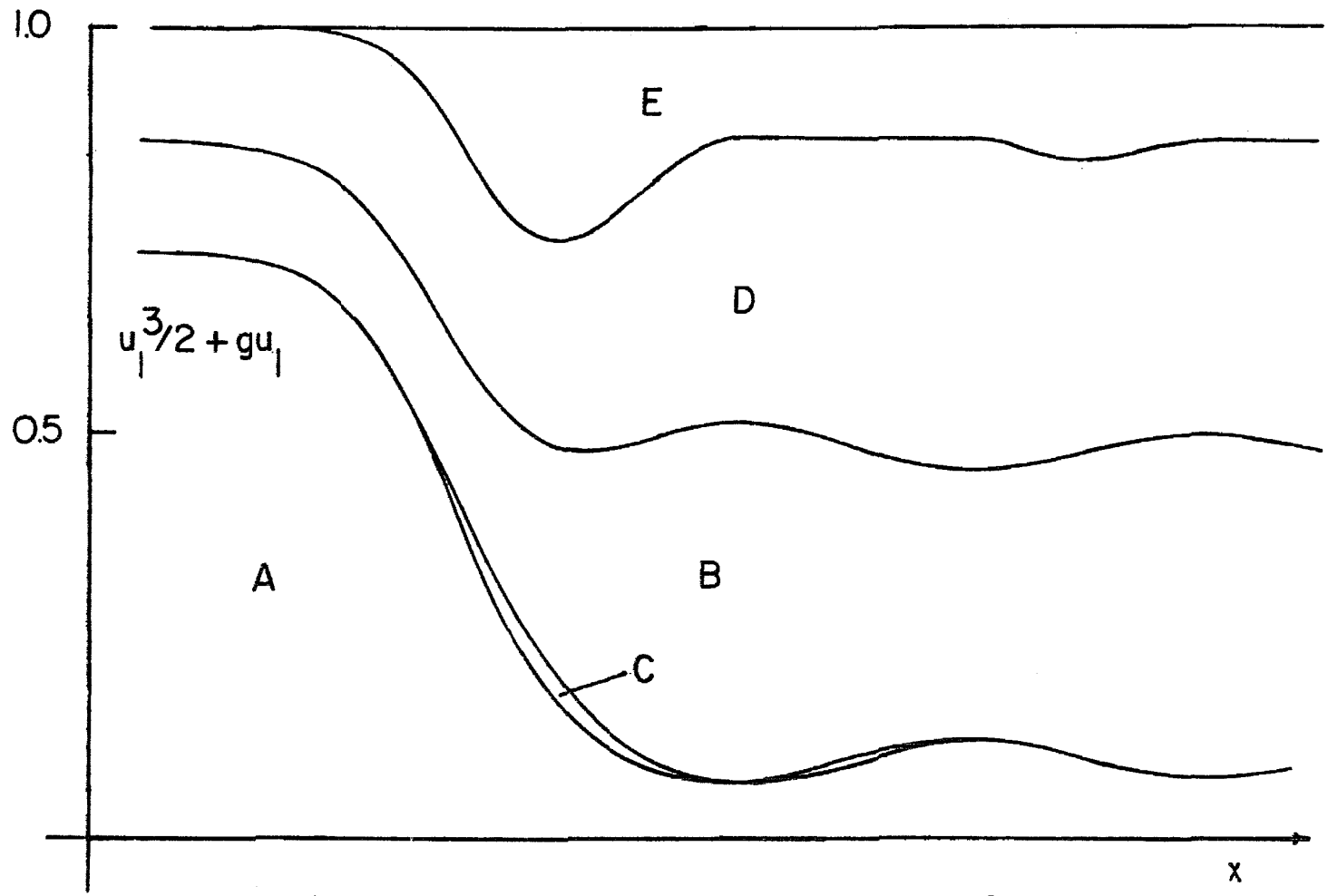

Figure 5 (c) - Energy terms for shock with Fr = 2.3 and a^2 = 1.0.

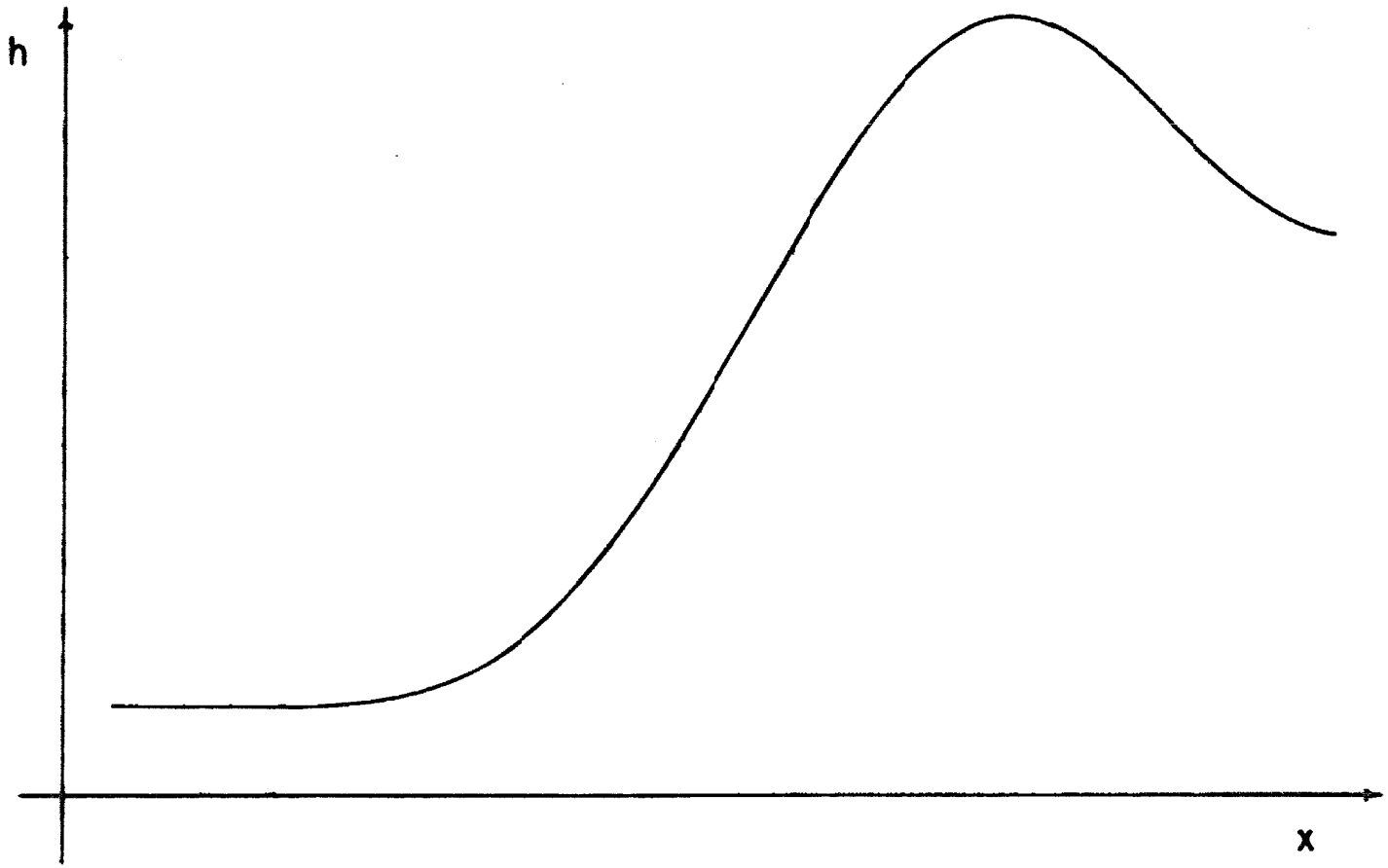

Figure 6 (a) - Profile of shock with Fr = 5.7 and a^3 = 1.0.

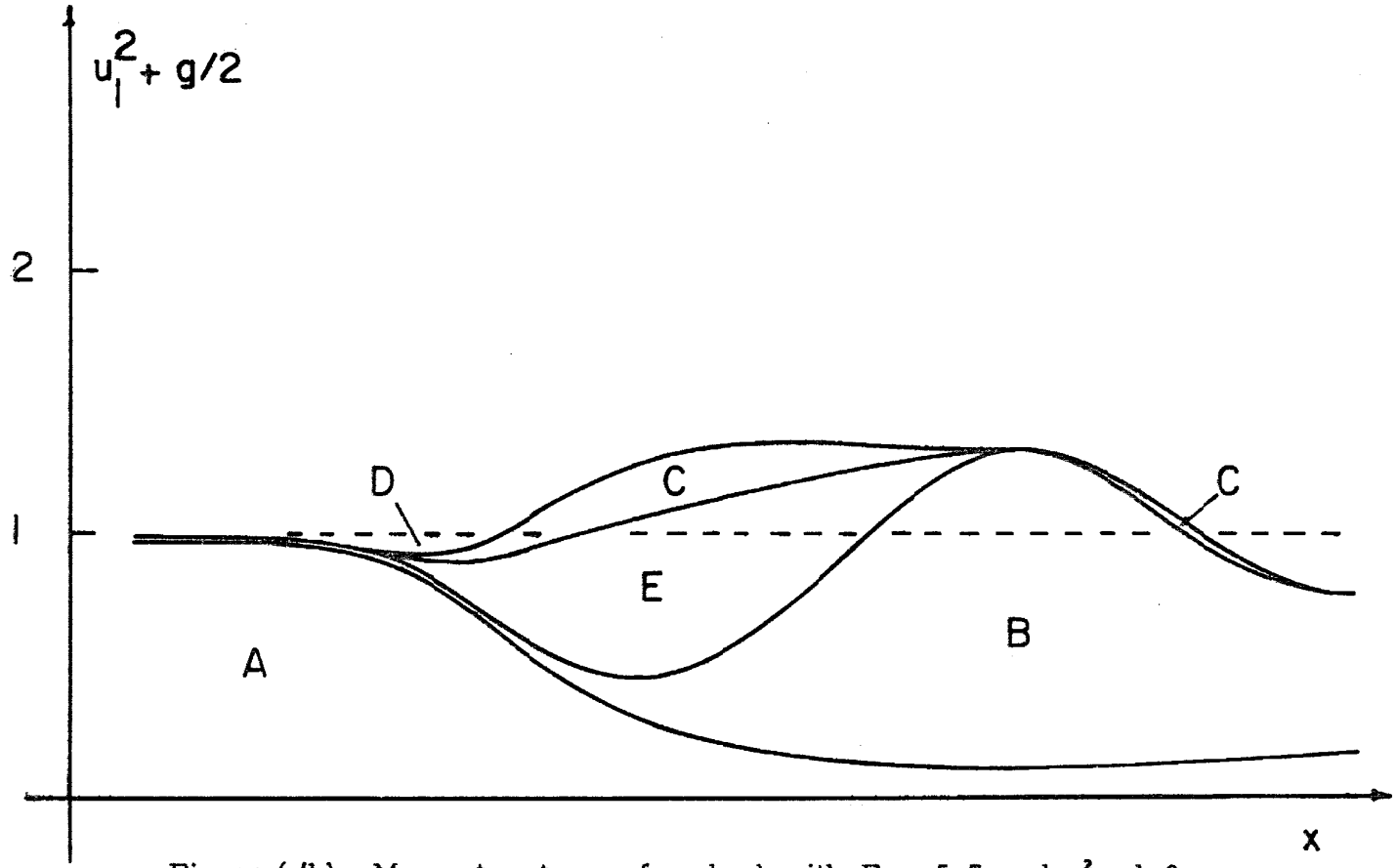

Figure 6 (b) - Momentum terms for shock with $Fr = 5.7$ and $a^2 = 1.0$.

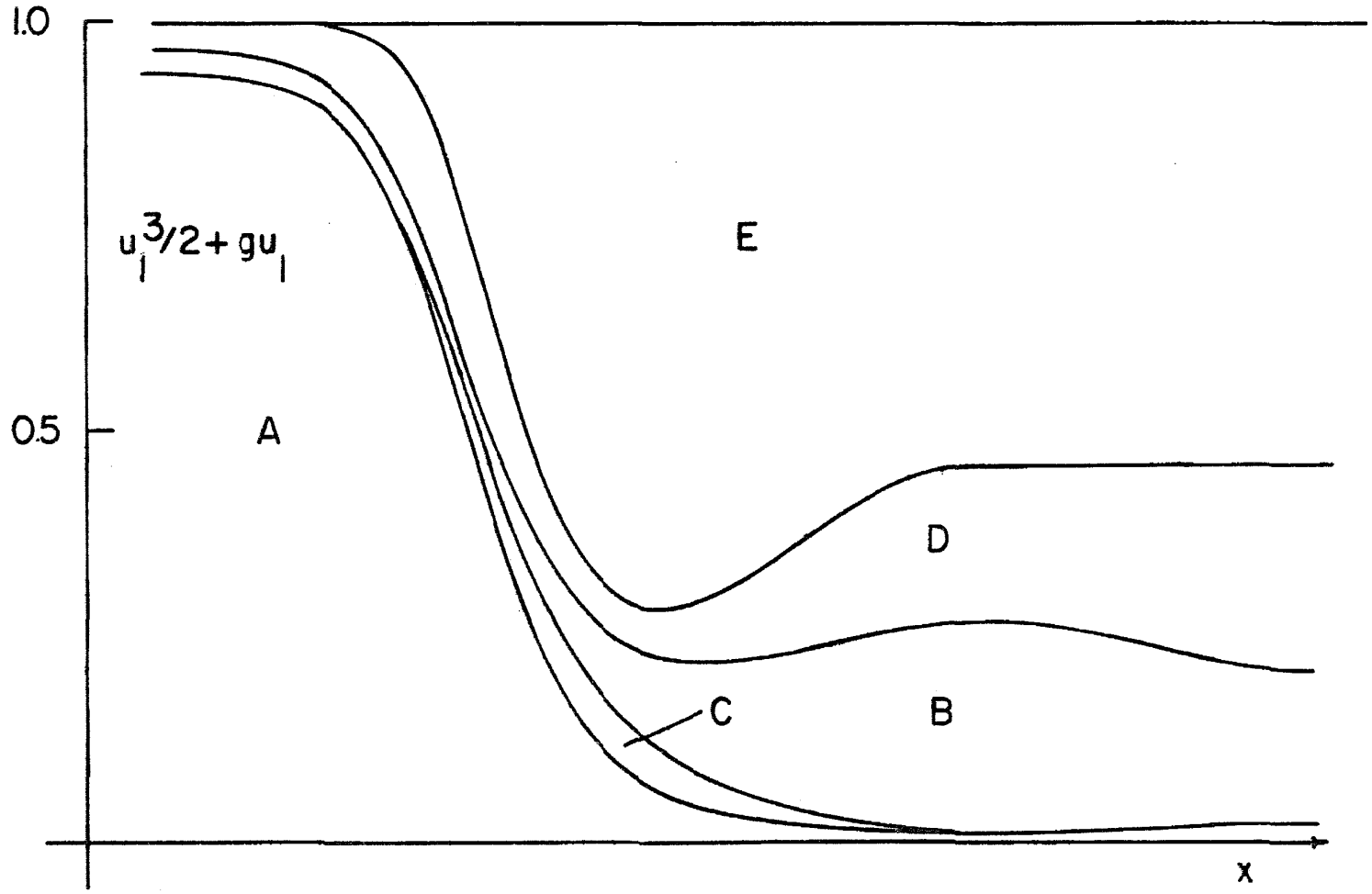

Figure 6 (c) - Energy terms for shock with $Fr = 5.7$ and $a^2 = 1.0$.

Once the solutions for ths shock are obtained, the question arises: How do the solutions obtained compare with the behavior of the actual shocks formed in the run-up flow? Experimental data on steady shocks (hydraulic jump) summarized by Ven Te Chow (1) is used as a basis for comparison. Figure 7 summarizes the results of the experiments and the shock profile calculations. The dimensionless width of the shock, $\overline{L}$, is plotted vs. H, which is the height ratio across the shock (h_2/h_1) minus one. (If there is no shock, H = 0).

$\overline{L}$ is given by

$$\overline{L} = \frac{L}{h_2 - h_1}$$

where L is defined as the maximum slope width, as illustrated in Figure 8. It can be seen that the calculated shocks tend to be narrower than the experimental ones for some reasonable value of a^2, i.e., $a^2 = 1.0$. However, this alone does not seem to be a serious problem.

Damping Due to Artificial Viscosity Term

A larger drawback of the artificial viscosity term is that it tends to remove energy from waves where no shock has formed and ideally there are no losses. This can be seen in Figure 9 which summarizes calculations for the propagation of a solitary wave, initially generated with an H/d = 0.5. It shows the decrease in amplitude vs. the dimensionless distance L/d the wave has traveled. (H is wave height, d is depth, and L is length of travel). For higher values of a^2 the wave rapidly decays.

As a basis for comparison, consider the solitary wave in an experimental model tank with a depth of one foot and a height of one-half foot (H/d = 0.5) traveling one hundred feet (L/d = 100). It decays due to

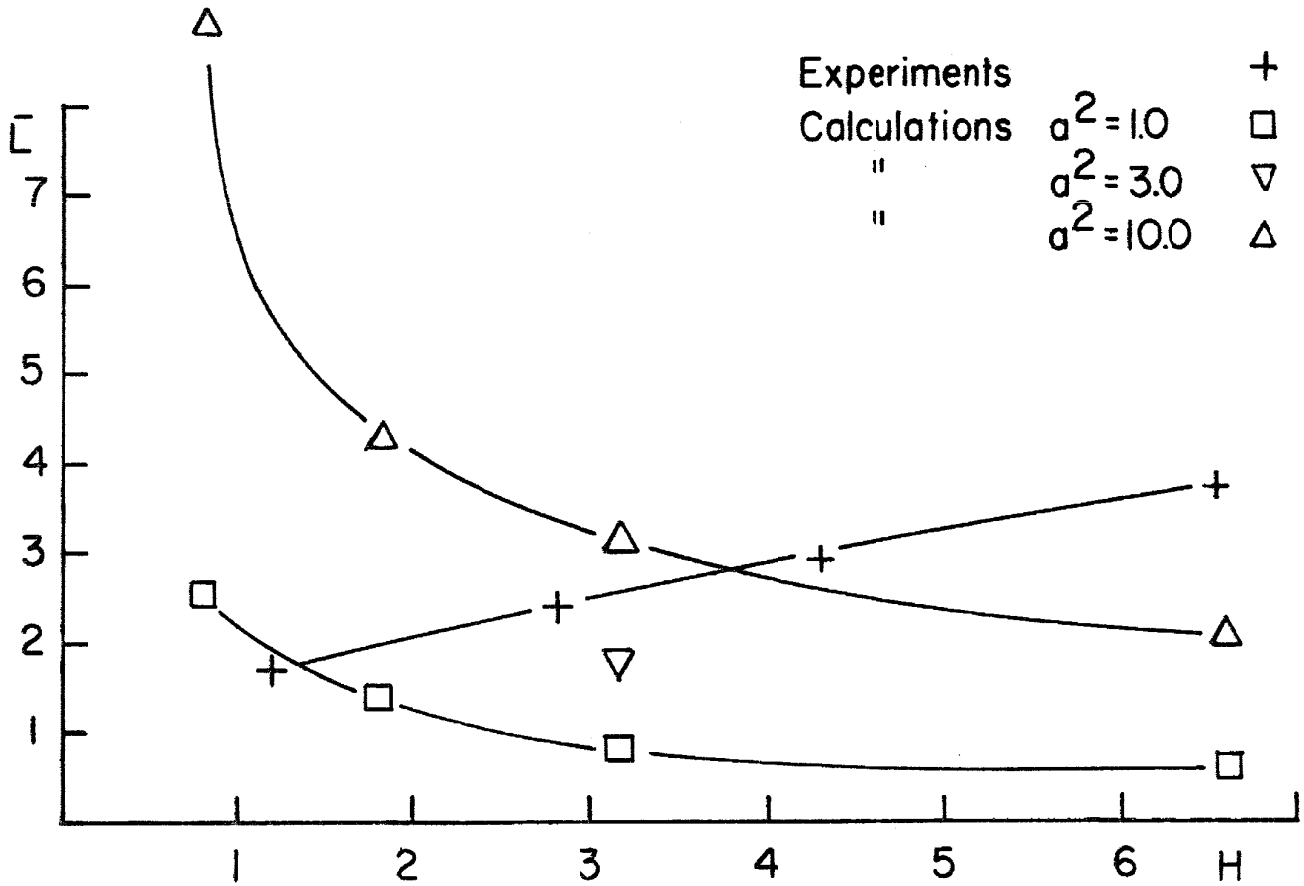

Figure 7 - Behavior of shock width vs. height ratio, comparing experimental measurements and calculated solutions.

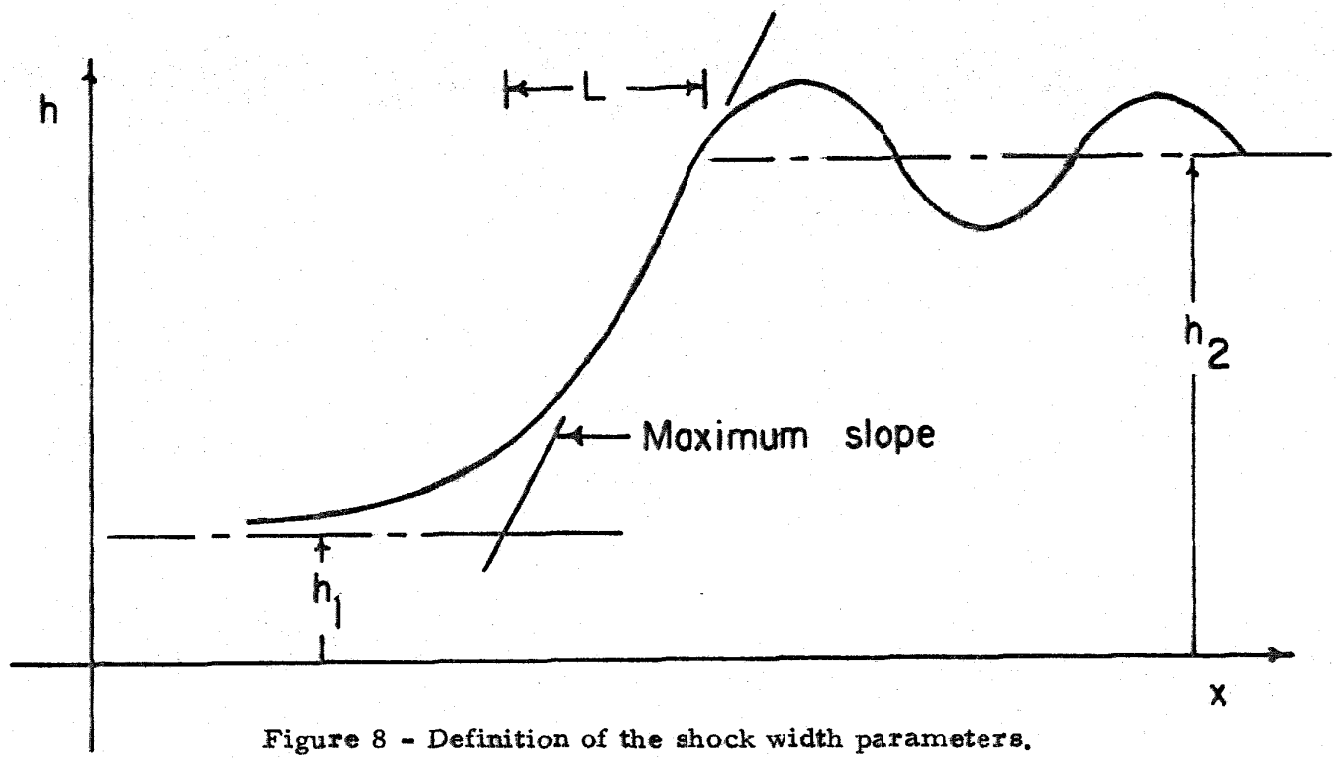

Figure 8 - Definition of the shock width parameters.

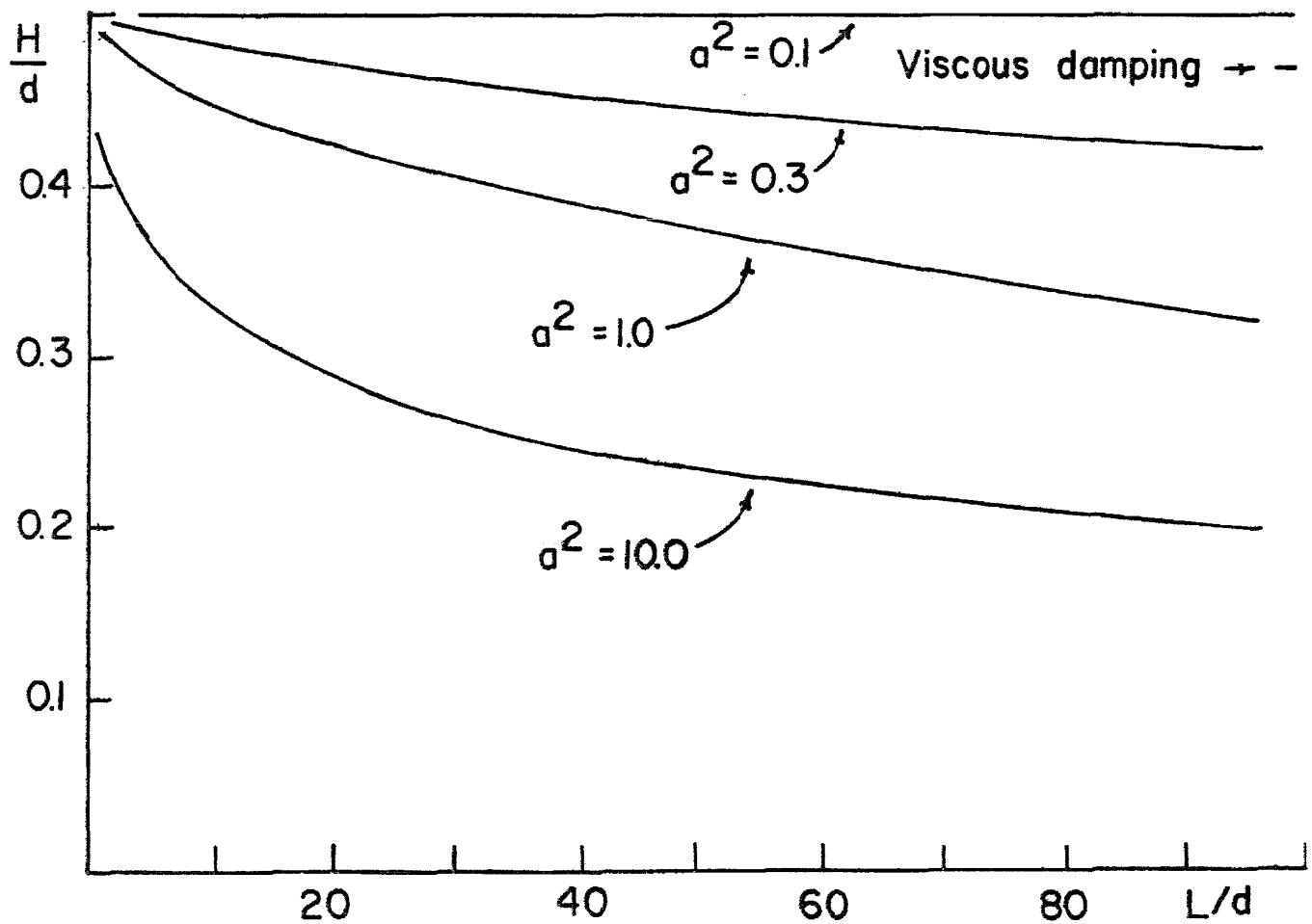

Figure 9 - Decay of solitary waves due to the artificial viscosity term.

viscous damping. This decay can be calculated from a formula given by Keulegan (3) and is indicated by the level marked "Viscous Damping" at L/d = 100 on Figure 9. For a larger experimental model, this level would be even higher, i.e., very little natural attenuation of the wave would occur. Hence, it can be seen that the present artificial viscosity term causes excessive damping of solitary waves.

An easy method of dealing with the problem is to try to pick a compromise value of a^2 which gives reasonable modeling of the shock, and yet does not cause excessive attenuation of solitary waves. However, this would require constant re-examining of the solutions to make sure some phenomena was not being improperly represented.

Use of Variable Coefficient Artificial Viscosity Term

A better method, however, is to consider a^2 as a variable. Ideally, it would be zero for solitary waves and undular bores, where no energy dissipation is taking place (in turbulent rotational flow of the fluid). Only for stronger bores would a^2 increase so as to provide a high level of internal energy dissipation.*

A general approach to this seems to be to replace a^2 by a function G( ), which would vary to provide the correct level of dissipation for the phenomena occurring. The argument of G( ) would have to be some combination of the flow variables that would indicate what was occurring.

The velocity gradient u_x is one indicator of the nature of the flow. It becomes large (negatively) when the flow steepens into a shock, but is smaller for other phenomena, such as solitary waves. Since u_x has dimensional units, it will vary with the choice of scale size. This can be eliminated by using the depth h to cancel the length dimension and the

*The simplest possibility here is the use of a step function which would be zero for solitary waves and undular bores, and non-zero for shocks.

small amplitude wave speed $\sqrt{gh}$ to cancel the velocity, giving $u_x h/\sqrt{gh} = u_x\sqrt{h/g}$ as a candidate for the argument of G( ).

It is also important that this argument be invariant under a Galilian transformation, so that the equation is valid in any reference frame moving at constant velocity. As an example of this suppose u_x had been non-dimensionalized by using u, the horizontal velocity to cancel the velocity dimension. The argument $u_x \frac{h}{u}$ is non-dimensional, but not invariant. If the reference frame is moving so that $u \to 0$, the argument becomes large even if no shocks are present. However, the qualities u_x and h are invariant, so their use in the form $u_x\sqrt{h/g}$ as the argument of G( ) gives a result independent of the reference frame. (Another possible candidate for the argument of G( ) is h_x).

(See Appendix E for a discussion of invariance under Galilian transformation).

Hence, the momentum equation is rewritten as

$$(uh)_t + \left\{ u^2 h + \tfrac{1}{2} gh^2 + \tfrac{1}{3} h^3 (u_x{}^2 - u_{xt} - u_{xx}) + G\,(u_x\sqrt{h/g})\, u_x{}^2 h^3 \right\}_x = 0 \qquad (12)$$

where $G(u_x\sqrt{h/g})$ has been substituted for a^2 in equation (2).

The form of G can be determined from knowledge of how the artificial viscosity term should behave. Since $h > 0$ (always), if $u_x > 0$, then $u_x\sqrt{h/g} > 0$. However $u_x > 0$ for rarefraction waves where no dissipation takes place, so $G = 0$ for $(u_x\sqrt{h/g}) > 0$. (This is the same task done by the function Hysd( ) for the constant coefficient artificial viscosity term.)

For $u_x < 0$, the picture is more complicated. An approximate calculation of G( ) from known experimental data for shock behavior is done in Appendix D. This gives some indication of the requirements for G( ). For undular bores it is found $G = 0$ for $0 < u_x \sqrt{h/g} < .67$. Naturally with $G = 0$, no energy is dissipated and the surplus energy of the shock is radiated downstream as additional waves. For stronger bores, (higher Froude numbers) where turbulent flow dissipates all the excess energy of the shock, the experimental data requires G ( ) to behave as shown by the dotted line in Figure 10. However, it can be seen that this approximate calculation has required G ( ) to be multi-valued. This is impossible to use in a real calculation because there is no way of telling which branch of the function should be used. A single-valued substitute would have to be found that would perform in roughly the same way.

To keep solitary wave damping small G would have to be small ($G < 0.1$) for the values of $u_x \sqrt{h/g}$ occurring in solitary waves. Table I indicates that $u_x \sqrt{h/g} > -2$ for solitary waves, so $G < 0.1$ in this region. For smaller $u_x \sqrt{h/g}$, G should increase rapidly to approximate the curve derived in Appendix D. It was observed that

$$G(\ ) = \begin{cases} 100(\ )^4 & (\ ) \leq 0 \\ 0 & (\ ) > 0 \end{cases} \qquad (13)$$

seem to fit these requirements and so it was tested.

Figures 11-14 show profiles of shocks with different Froude numbers calculated to be solving the shock equations using (13). For Fr = 1.6 the behavior of the shock is almost undular with relatively large downstream waves. For the stronger shocks, only a very small

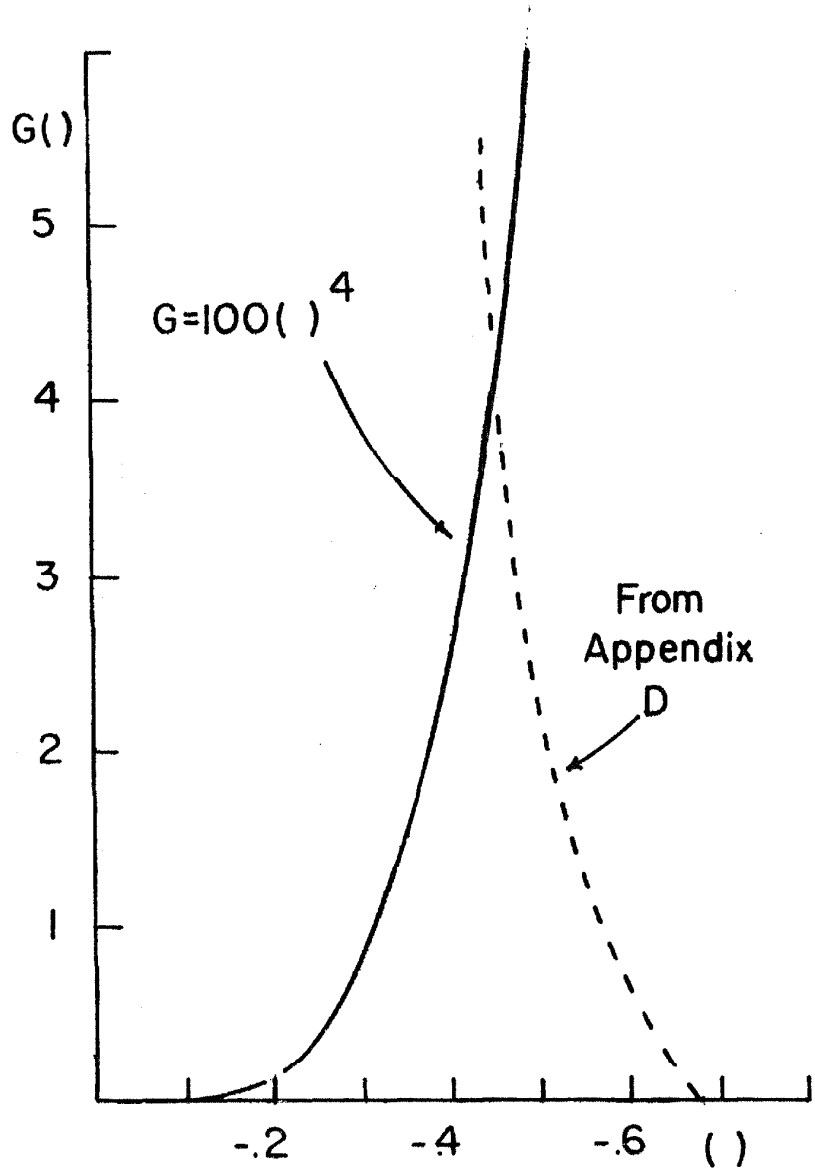

Figure 10 - Plot of G ($u_x \sqrt{h/g}$)

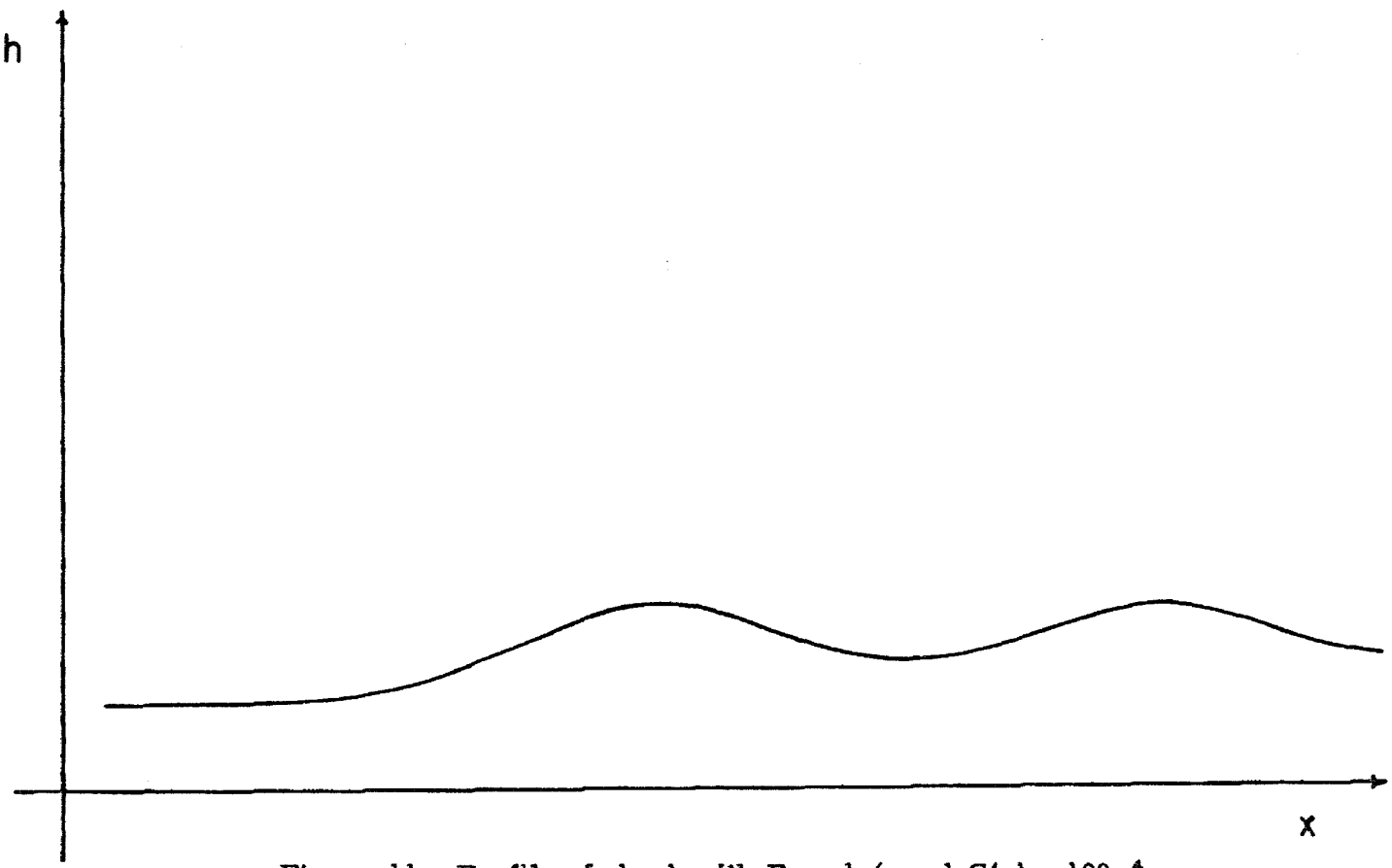

Figure 11 - Profile of shock with Fr = 1.6 and $G(x) = 100x^4$.

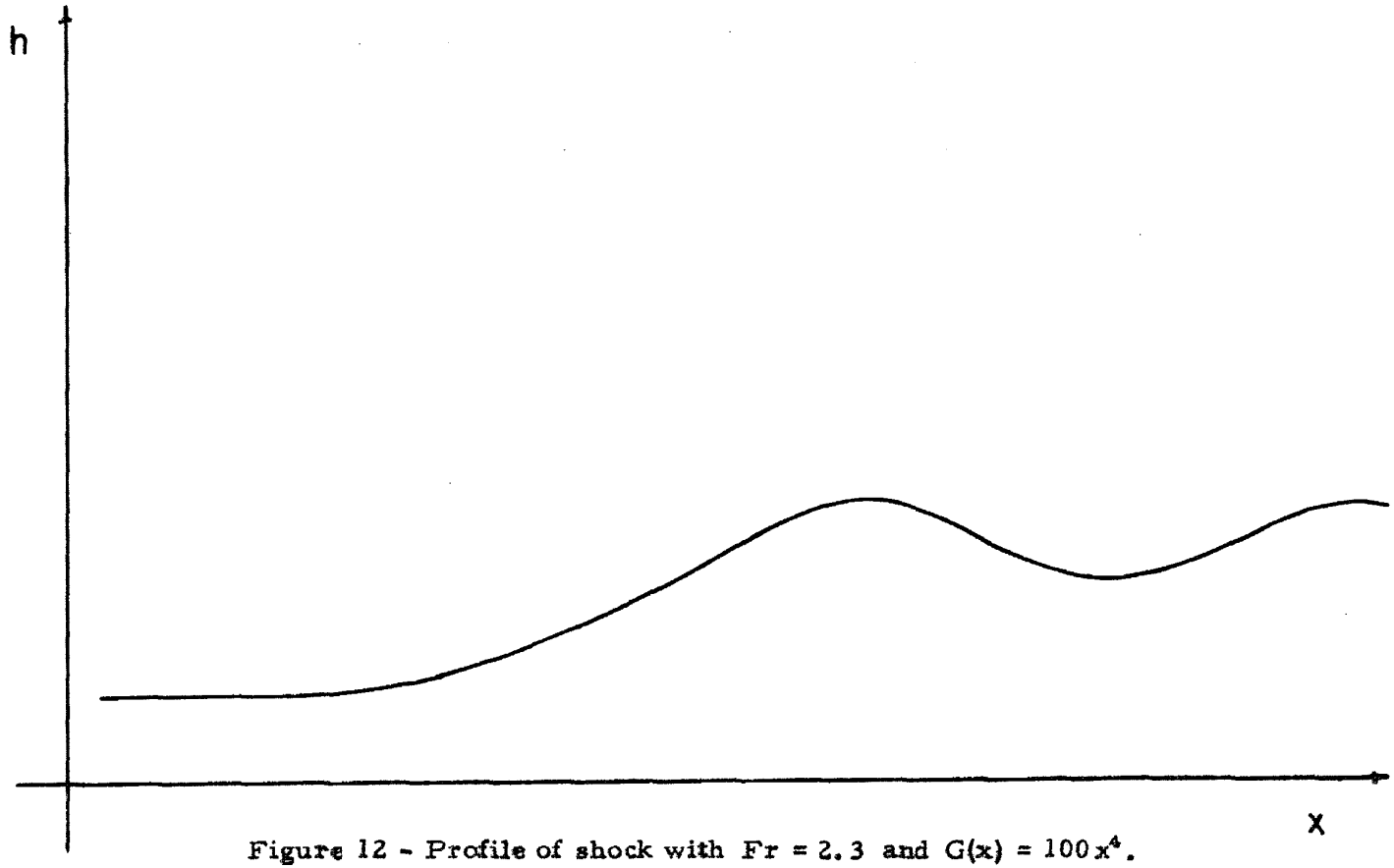

Figure 12 - Profile of shock with Fr = 2.3 and $G(x) = 100x^4$.

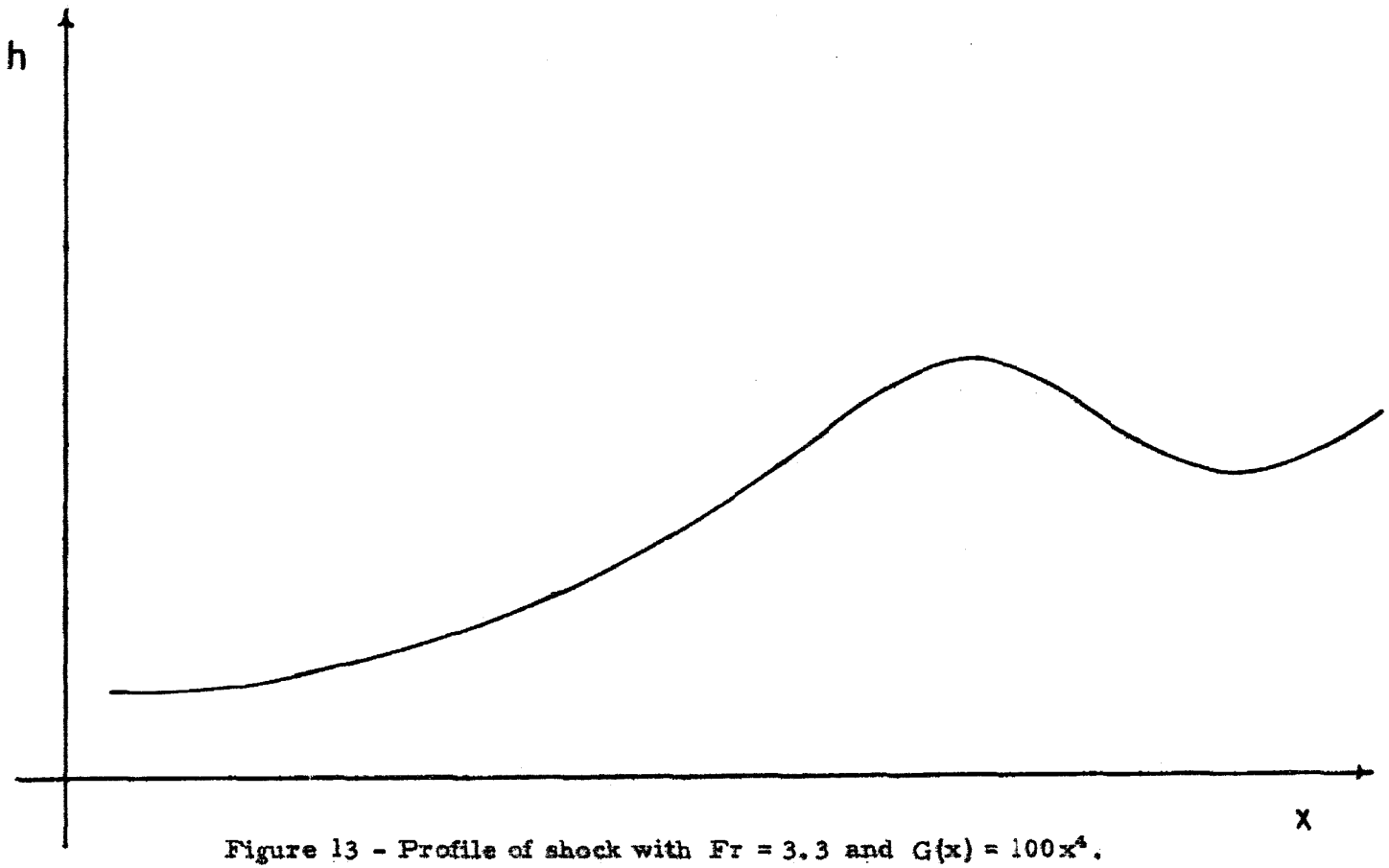

Figure 13 - Profile of shock with $Fr = 3.3$ and $G(x) = 100x^4$.

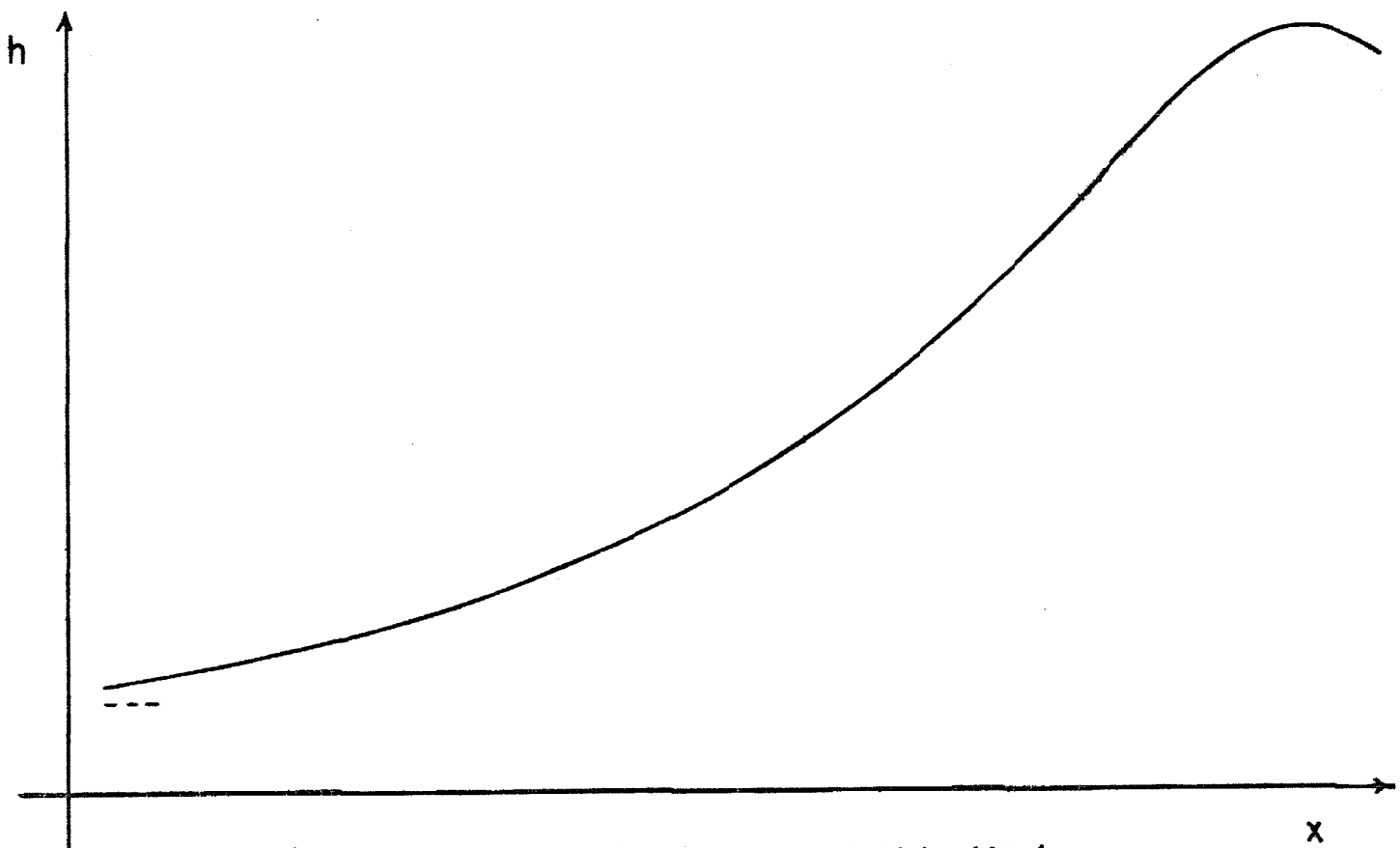

Figure 14 - Profile of shock with $Fr = 5.7$ and $G(x) = 100x^4$.

amount of downstream undulation is observed, with most of the energy being dissipated.

A solitary wave with $H/d = 0.5$ initially was allowed to propagate for $L/d = 100$ using (13). No attenuation was noticeable.

TABLE I

Solitary Wave	Maximum Value of
H/d	$u_x\sqrt{h/g}$
.70	-.164
.72	-.1645
.78	-.1653

Conclusions

It can be seen that the artificial viscosity term can be improved to give more realistic results for the behavior of both undular and strong bores. Hence, the model can give improved results for run-up flows where bore formation occurs. A consequence of this is that no undue damping of solitary (or other finite amplitude) waveforms takes place.

In addition, calculation of the individual terms in a shock profile shows that the use of the artificial viscosity term is necessary to remove the energy dissipated in the shock, and prevent its radiation downstream. Without an artificial viscosity term, that is $G(\ ) = 0$, all shocks are undular and radiate waves downstream.

The evolution of more sophisticated methods of modelling the shock flow is limited at this point by the basic assumption of the constrained flow, i.e., the horizontal velocity is independent of depth. To

really get the shock behavior in detail, two-dimensional flow would have to be considered, with the need for much larger computational schemes and computing costs. However, for the modelling of many run-up flow problems, the use of the artificial viscosity term with the G( ) function seems to provide an adequate model.

REFERENCES

1. Chow, V. T., "Hydraulic Jump and Its Use as Energy Dissipator," Open Channel Hydraulics, McGraw-Hill, New York, 1959, p. 400

2. Heitner, K. L. "A Mathematical Model for Calculation of the Run-Up of Tsunamis," Thesis presented to the California Institute of Technology, Pasadena, California, 1969 in partial fulfillment of the requirements for the degree of Doctor of Philosophy.

3. Keulegan, G. H., "Gradual Damping of Solitary Waves," J. of Research, National Bureau of Standards, Vol. 40, Paper RP-1895, June, 1948, pp. 487-98.

4. Von Neumann, J., and Richtmyer, R. D., "A Method for Numerical Calculation of Hydrodynamic Shocks," Journal of Applied Physics, Vol. 21, March, 1950, pp. 232-237.

APPENDIX A

Similarity Solutions for Shocks Using the Artificial Viscosity Term

The objective of this appendix is to show that the solutions to the shock equations are only a function of the Froude number of the shock Fr and the artificial viscosity coefficient a^2.

Consider first the equations of motion for a constrained flow, using the simple artificial viscosity term of the form $a^2 h^3 (u_x)^2 \text{Hysd}(-u_x)$ where a is the dimensionless shock coefficient, h the depth, u the horizontal velocity, and x the horizontal independent space variable, and

$$\text{Hysd}(x) = \begin{Bmatrix} 0 & x \le 0 \\ 1 & x > 0 \end{Bmatrix} \tag{A-1}$$

The equations of motion are

$$h_t + (uh)_x = 0$$

$$(uh)_t + \Big(u^2 h + \tfrac{1}{2} g h^2 + \tfrac{1}{3} h^3 \, (u_x{}^2 - u_{xt} - u u_{xx}) + a^2 h^3 (u_x)^2 \, \text{Hysd}\,(-u_x) \Big)_x = 0 \tag{A-2}$$

where t is time.

Examining the equations in the reference frame moving with the shock, the flow is steady and the derivatives with respect to time are zero. Using the upstream values of $u = u_1$ and $h = h_1$, the equations may be integrated once to give

$$uh = u_1 h_1$$

$$u^2 h + \tfrac{1}{2} g h^2 + \tfrac{1}{3} h^3 \left(\left(\frac{du}{dx} \right)^2 - u \, \frac{d^2 u}{dx^2} \right) + a^2 h^3 \left(\frac{du}{dx} \right)^2 \text{Hsyd} \left(- \frac{du}{dx} \right) = u_1{}^2 h_1 + \tfrac{1}{2} g h_1{}^2 \tag{A-3}$$

If we define dimensionless variables

$$u^* = \frac{u}{u_1} \qquad h^* = \frac{h}{h_1} \qquad x^* = \frac{x}{h_1}$$

$$\frac{du^*}{dx^*} = \frac{du}{dx}\left(\frac{h_1}{u_1}\right) \qquad \frac{d^2u^*}{dx^{*2}} = \frac{d^2u}{dx^2}\,\frac{h_1^2}{u_1} \tag{A-4}$$

Then the equations become,

$$u^* h^* = 1$$

$$(u^* u_1)^2\, h^* h_1 + \tfrac{1}{2} g\,(h^* h_1)^2 +$$

$$\tfrac{1}{3}(h_1 h^*)^3 \left(\left(\frac{du^*}{du^*}\right)^2 \left(\frac{u_1}{h_1}\right)^2 - u^* \frac{d^2u^*}{dx^{*2}} \left(\frac{u_1}{h_1}\right)^2\right) +$$

$$a^2 (h_1 h^*)^3 \left(\frac{du^*}{dx^*}\right)^2 \left(\frac{u_1}{h_1}\right)^2 \text{Hysd}\left(-\frac{du^*}{dx^*}\left(\frac{u_1}{h_1}\right)\right) = u_1^2 h_1 + \tfrac{1}{2} g h_1^2 \tag{A-5}$$

Noting that the Froude number Fr is defined by

$$Fr = \frac{u_1}{\sqrt{g h_1}} \tag{A-6}$$

the equations can be rearranged

$$u^* h^* = 1$$

$$(u^*)^2 h^* + \frac{g(h^*)^2}{2Fr^2} + \frac{1}{3}(h^*)^3 \left(\left(\frac{du^*}{dx^*}\right)^2 - u^* \frac{d^2u^*}{dx^2}\right)$$

$$+ a^2 (h^*)^3 \left(\frac{du^*}{du^*}\right)^2 \text{Hysd}\left(-\frac{du^*}{dx^*}\right) = 1 + \frac{1}{2Fr^2} \tag{A-7}$$

These equations are dimensionless and the only parameters involved in the solution are the Froude number Fr and the coefficient a^2. Hence, the solution is independent of the choice of dimensions for the variables.

If the nature of the artificial viscosity term is generalized so that a^2 is replaced by a function

$$G\left(\frac{du}{dx}\sqrt{\frac{h}{g}}\right),$$

then in the new variables the argument become

$$\frac{du}{dx}\sqrt{\frac{h}{g}} = \frac{u_1}{h_1}\frac{du^*}{dx^*}\sqrt{\frac{h_1\,h^*}{g}} = \frac{u_1}{\sqrt{gh_1}}\frac{du^*}{dx^*}\sqrt{h^*}$$

$$= Fr\,\frac{du^*}{dx^*}\sqrt{h^*}$$

Hence, again only the Froude number enters into the solution which will be determined regardless of dimensions if Fr and G( ) are specified.

APPENDIX B

Stability of the Shock Solution

In obtaining solutions for a steady shock, the initial conditions from the upstream side of the shock are used to start the integration of the flow equations to the downstream side. It is desired to know if this integration will converge on the downstream side of the shock to the proper downstream conditions.

This can be seen by examining the governing equations in the "phase" plane. The basic equations

$$uh = u_1$$

$$u^2h + \tfrac{1}{2}gh^2 + \tfrac{1}{3}h^3\left((u')^2 - uu''\right) + a^2h^3(u')^2 \,\mathrm{Hysd}\,(-u')$$
$$= u_1^2 + g/2 \qquad \text{(B-1)}$$

are rearranged in the form

$$\frac{du'}{du} = \frac{Q(u) - (u')^2 P(u_1, u')}{2u'} \qquad \text{(B-2)}$$

where

$$Q(u) = \frac{6}{u_1^2}(u - u_1)\left(u^2 - \frac{gu}{2u_1} - \frac{g}{2}\right)$$

$$P(u_1, u') = -\frac{2}{u} - \frac{6a^2u}{u_1^2}\,\mathrm{Hysd}\,(-u') \qquad \text{(B-3)}$$

Figure B1 shows the "phase" plane plot for equations (B-2) and (B-3) drawn by a computer controlled plotter. The trajectories are represented by short tangents placed on a rectangular grid. (This is easier than trying to draw the actual trajectories). Also plotted is the shock solution shown as a solid line.

The plot shows the tendency of the solution to converge on the downstream value of u. All of the equation trajectories converge on

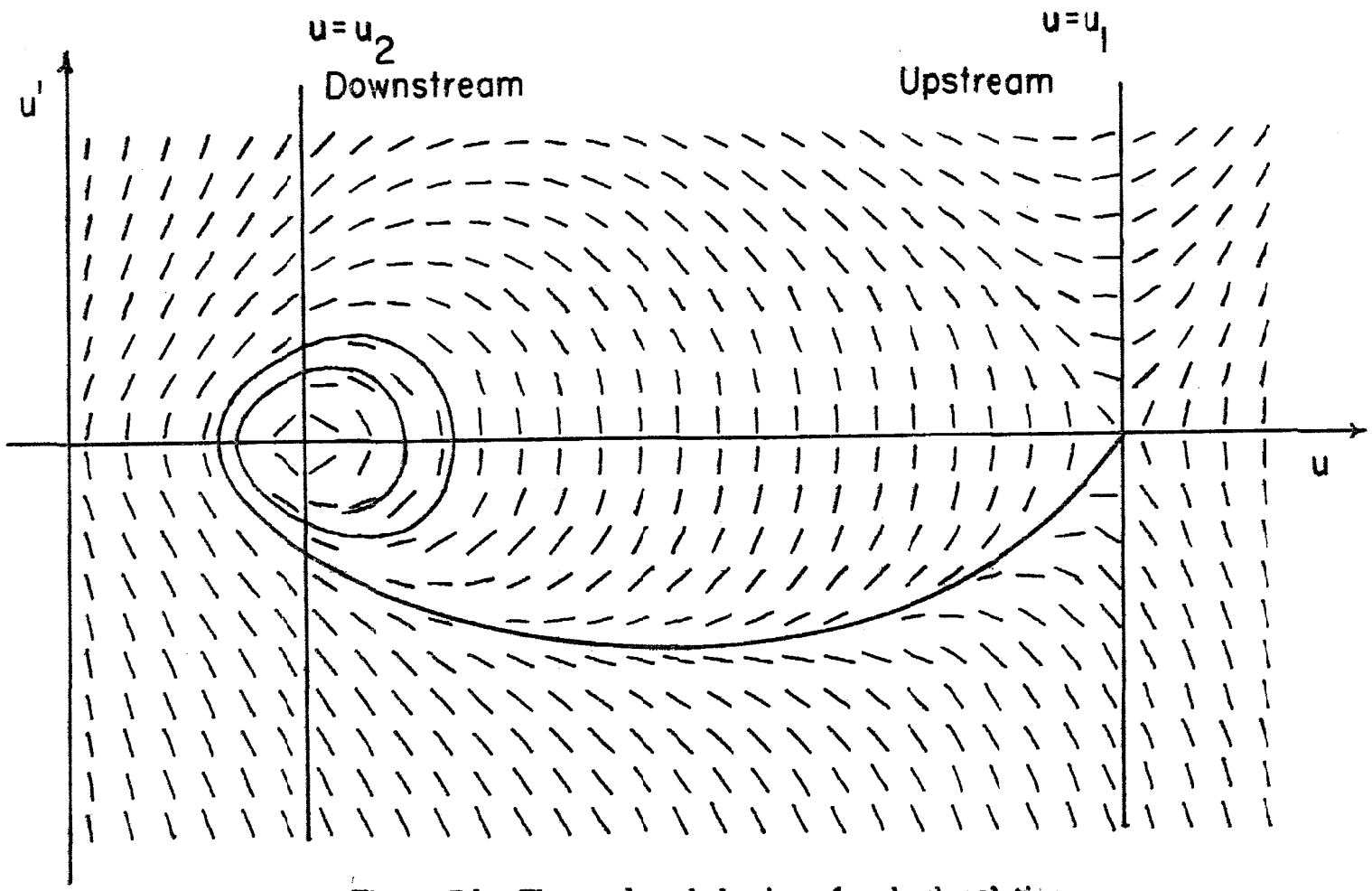

Figure B1 - Phase plane behavior of a shock solution.

the solution trajectory in the direction of integration indicating the solution is stable.

This means that any small error in the initial conditions near $u = u_1$ will not be important since the trajectory from the perturbed initial point will converge with that of the original initial point to the same solution downstream.

APPENDIX C

The Energy Equation With an Artificial Viscosity Term

The objective of this appendix is to give a complete discussion of the energy equation for the constrained flow, including the energy dissipation resulting from the use of an artificial viscosity term. The results will allow the individual terms of the energy equation to be calculated explicitly, so that the shock solution can be checked for energy balance.

For an element of fluid in a constrained flow, (see Figure C-1), its total energy consists of

a) Horizontal kinetic energy = $\frac{u^2 h}{2} dx$

b) Potential energy = $\frac{gh^2}{2} dx$

(where h = 0 is the reference plane)

c) Vertical kinetic energy = $\int_0^h \frac{v^2}{2} dydx$

Here, u is the horizontal velocity, v the vertical velocity, and h is the depth. Since u is not a function of y (in the constrained flow), the continuity equation

$$u_x + v_y = 0 \tag{C-1}$$

is integrated to give

$$u = - yv_x \tag{C-2}$$

since v = 0 at y = 0. This allows the vertical kinetic energy to be evaluated

$$V.K.E. = u_x^{\,2} h^3/6 \tag{C-3}$$

The total energy density E, is given by

$$E = \frac{u^2 h}{2} + \frac{gh^2}{2} + u_x^{\,2} \frac{h^3}{6} \tag{C-4}$$

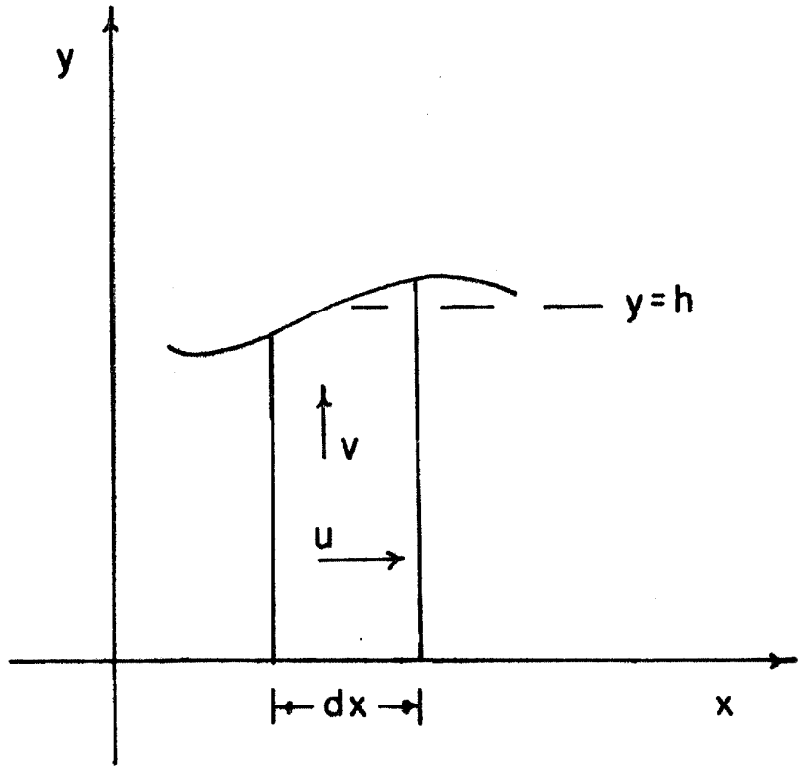

Figure C1 - An element of fluid in a constrained flow.

The total pressure force P on a vertical cross section is given by

$$P = \frac{gh^2}{2} + \frac{h^3}{3}\left(u_x^2 - u_{xt} - uu_{xx}\right) \tag{C-5}$$

See Heitner (2). The energy equation for a section between x_1 and x_2 may be written as

$$\frac{d}{dt}\int_{x_1}^{x_2} dE + \underbrace{\left[uE\right.}_{\text{Trans-port}} + \underbrace{\left.Pu\right]_{x_1}^{x_2}}_{\text{Boundary Work}} + \underbrace{\int_{x_1}^{x_2} dD}_{\text{Dissipation}} = 0 \tag{C-6}$$

where D is the energy dissipation density.

In differential form this is

$$E_t + \left[u\,(E + P)\right]_x + D = 0 \tag{C-7}$$

When solved with the continuity and momentum equations for the constrained flow, i.e.,

$$h_t + (uh)_x = 0$$

$$(uh)_t + (u^2h + P + F)_x = 0 \tag{C-8}$$

the relation between the energy dissipation density D and the artificial viscosity force F is found to be

$$D = F_x u \tag{C-9}$$

When a shock solution is examined in a coordinate system fixed to the shock, the flow is steady and the energy equation becomes

$$\left[u\,(E + P)\right]_x + D = 0 \tag{C-10}$$

Integrating with respect to x and denoting the upstream conditions $u = u_1$, $E = E_1$, $P = P_1$, $D = 0$, the energy equation becomes

$$u\,(E + P) + \int D dx = (E_1 + P_1)u_1$$

$$u\,(E + P) + \int F_x u\, dx = (E_1 + P_1)u_1 \qquad \text{(C-11)}$$

Substituting the expressions for E, P, F, etc. gives:

$$u\left(\frac{u^2 h}{2} + \frac{gh^2}{2} + u_x^2\,\frac{h^3}{6} + \frac{gh^2}{2} + \frac{h^3}{3}\,(u_x^2 - uu_{xx})\right) +$$

$$\int u\left(a^2 h^3\, u_x^2\, \mathrm{Hysd}\,(-u_x)\right)_x dx = \frac{u_1^3}{2} + u_1 g \qquad \text{(C-12)}$$

where D has been taken as

$$D = a^2 h^3 u_x^2\, \mathrm{Hysd}\,(-u_x) \qquad \text{(C-13)}$$

All derivatives with respect to time are zero.

APPENDIX D

Approximate Calculation of Artificial Viscosity Term for Shocks

If the artificial viscosity term has a variable coefficient $G\left(u_x\sqrt{h/g}\right)$, the problem is to determine G ( ) so the shock behavior agrees with experimental data. Some insight into the nature of G ( ) can be gained by an approximate solution for the shock, allowing G ( ) to be found in terms of the experimental results.

The equations governing the constrained flow with a variable coefficient artificial viscosity term are

$$h_t + (uh)_x = 0$$

$$(uh)_t + \left\{ u^2 h + \tfrac{1}{2} g h^2 + \tfrac{1}{3} h^3 \left(u_x^2 - u_{xt} - u u_{xx} \right) + G\left(u_x \sqrt{\frac{h}{g}} \right) h^3 u_x^2 \right\}_x = 0 \qquad \text{(D-1)}$$

These equations are valid for a coordinate system moving at any fixed speed. Fixing the coordinates to a shock, the flow appears steady and the flow quantities are functions of x only, i.e. $h = h(x)$, $u = u(x)$, giving

$$(uh)' = 0$$

$$\left(u^2 h + \tfrac{1}{2} g h^2 + \tfrac{1}{3} h^3 \left((u')^2 - u u'' \right) + G\left(u' \sqrt{\frac{h}{g}} \right) h^3 (u')^2 \right)' = 0 \qquad \text{(D-2)}$$

as two O.D.E.'s to be solved. These can be integrated to give

$$A + uh = 0$$

$$B + u^2 h + \tfrac{1}{2} g h^2 + \tfrac{1}{3} h^3 \left((u')^2 - u u'' \right) + G\left(u' \sqrt{\frac{h}{g}} \right) h^3 (u')^2 = 0 \qquad \text{(D-3)}$$

where A and B are constants. For a shock-like solution, it is desired that far away from the shock (centered at $x = 0$), the flow quantities become constant values. Hence, the following conditions are imposed.

As	$x \to -\infty$	$u \to u_1$	$h \to h_1$	$u' \to 0$	$u'' \to 0$
	$x \to +\infty$	$u \to u_2$	$h \to h_2$	$u' \to 0$	$u'' \to 0$

This leads to the shock conditions

$$u_1 h_1 = u_2 h_2$$

$$u_1^2 h_1 + \tfrac{1}{2} g h_1^2 = u_2^2 h_2 + \tfrac{1}{2} g h_2^2 \tag{D-4}$$

(assuming the function $G\left(u_x \sqrt{\frac{h}{g}}\right)$ is finite for finite arguments).

Equations (D-4) allows h_1 to be obtained in terms of u_1 and u_2

$$h_1 = \frac{2u_1 u_2^2}{g(u_1 + u_2)}$$

The constants A and B are evaluated

$$A = -u_1 h_1 = -\frac{2(u_1 u_2)^2}{g(u_1 + u_2)}$$

$$B = -(u_1^2 h_1 + \tfrac{1}{2} g h_2^2)$$

$$= -\left(\frac{2u_1^2 u_2^2 (u_1^2 + u_1 u_2 + u_2^2)}{g(u_1 + u_2)^2}\right) \tag{D-5}$$

Since

$$h = -A/u$$

the second equation of (D-3) can be rearranged

$$G\left(u'\sqrt{\frac{h}{g}}\right) h^2 (u')^2 + \tfrac{1}{3} h^2 \left((u')^2 - uu''\right)$$
$$+ u^2 + \tfrac{1}{2} gh + B/h = 0$$

$$G\left(u'\sqrt{\frac{h}{g}}\right)h^2(u')^2+\frac{1}{3}h^2\left((u')^2-uu''\right)=$$

$$(u_1-u)(u-u_2)\left[1+\frac{u_1u_2}{u(u_1+u_2)}\right] \qquad \text{(D-6)}$$

An approximate evaluation of the shock properties can be obtained by evaluating (D-6) at the average value of u and h, that is

$$u=\frac{u_1+u_2}{2} \qquad h=\frac{h_1+h_2}{2}$$

It is assumed that this is close to the inflection point in the shock profile, where the slope is a maximum, so that

$$u'=-\frac{u_1-u_2}{L} \qquad u''=0$$

where L is the slope width of the shock.

Substituting into (D-6)

$$\left(G\left(-\frac{u_1-u_2}{L}\sqrt{\frac{h_1+h_2}{2g}}\right)+\frac{1}{3}\right)\left(\frac{h_1+h_2}{2}\right)^2\left(\frac{u_1-u_2}{L}\right)^2=$$

$$\left(\frac{u_1-u_2}{2}\right)^2\left(1+\frac{2u_1u_2}{(u_1+u_2)^2}\right) \qquad \text{(D-7)}$$

The quantity $\left(1+2u_1u_2/(u_1+u_2)^2\right)$ varies between 1.0 and 1.25, so

$$G\left(-\frac{u_1-u_2}{L}\sqrt{\frac{h_1+h_2}{2g}}\right)+\frac{1}{3}\approx\left(\frac{L}{h_1+h_2}\right)^2 \qquad \text{(D-8)}$$

Using the first expression of (D-5) to give

$$\frac{1}{g}=\frac{u_1h_1(u_1+u_2)}{2(u_1u_2)^2}$$

(D-8) can be rearranged in terms of h_1, h_2, and L.

$$G\left(-\frac{h_2-h_1}{L}\cdot\frac{h_1+h_2}{2\sqrt{h_1h_2}}\right)+\frac{1}{3}\approx\left(\frac{L}{h_1+h_2}\right)^2 \qquad \text{(D-9)}$$

It is desirable to introduce two dimensionless variables

$$\bar{L} = \frac{L}{h_2 - h_1} \qquad H = \frac{h_2}{h_1} - 1$$

$\bar{L}$ is the nondimensional slope width of the shock, while H is the height ratio minus unity. Figure D1 shows the relation between $\bar{L}$ and H for turbulent bores where roller action is taking place. (This is from experimental data.)

For undular bores, G = 0, and

$$\left(\frac{L}{h_1 + h_2}\right)^2 \approx \frac{1}{3}$$

$$\bar{L} \approx \frac{1}{\sqrt{3}} \left(1 + \frac{2}{H}\right) \tag{D-10}$$

This curve is plotted on Figure D1 and shows how in the absence of any dissipation, the shock fronts tend to be excessively steep, (very small $\bar{L}$). (In addition, downstream of the shock, a wave train would be produced to carry off the undissipated energy.)

If expression (D-9) is rewritten as

$$\left(G\left(-\frac{1}{\bar{L}} \frac{H+2}{2\sqrt{H+1}}\right) + \frac{1}{3}\right)\left(\frac{H+2}{H}\right)^2 \approx (\bar{L})^2 \tag{D-11}$$

using the relation between H and $\bar{L}$ given by the experimental data for turbulent bores, G can be found. This is shown in Figure D-2 with the corresponding values of H for the turbulent region, i.e. H > 1.1.

For H < 1.1, the undular bore region where no energy dissipation is taking place, is represented by the line G = O. The

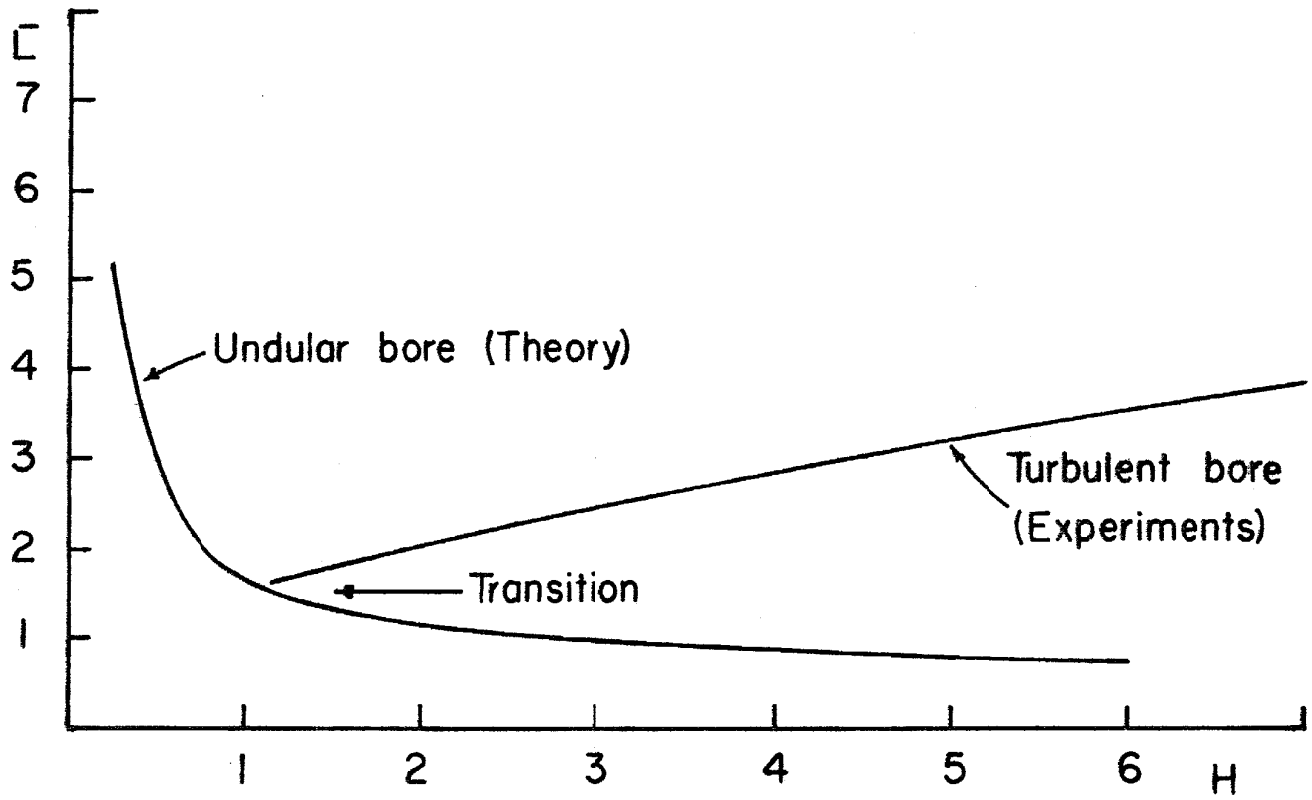

Figure D1 - Shock width vs. height ratio.

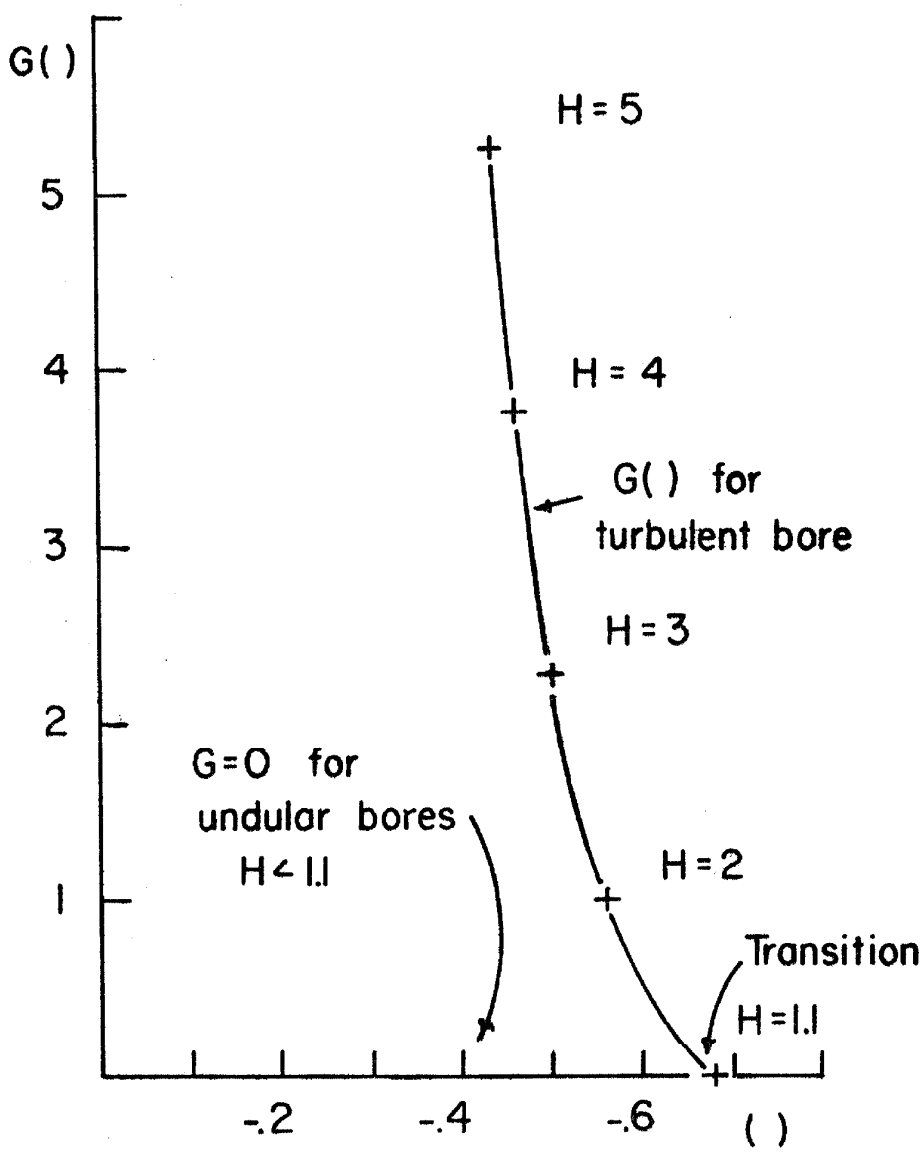

Figure D2 - Plot of G( ).

transition point between the undular bore and the turbulent bore is indicated on both plots.

APPENDIX E

Invariance Under Galilian Transformation

The idea that the equations of motion for the constrained flow were valid in any coordinate system has been used in several derivations. This appendix is an attempt to clarify this point, which is especially important in the choice of the argument for the variable artificial viscosity coefficient $G(u_x\sqrt{h/g})$.

If we consider two coordinate frames, one x and t, and the other $\tilde{x}$ and $\tilde{t}$, where x and $\tilde{x}$ are horizontal distance, and t and $\tilde{t}$ are times; then let the first system move horizontally at speed u_o with respect to the first. The time for both systems is considered simultaneous, i.e. $t = \tilde{t}$, but the horizontal distances are related $x = \tilde{x} + u_o t$.

Horizontal fluid velocities in the two systems differ by the relative velocity, i.e. $u = \tilde{u} + u_o$, but the height of the fluid free surface above the bottom is invarient $h = \tilde{h}$.

The properties of the partials of u and h can be established by equating total differentials, which are still invariant

$$dh = \frac{\partial h}{\partial x}\,dx + \frac{\partial h}{\partial t}\,dt = d\tilde{h}$$

$$= \frac{\partial \tilde{h}}{\partial \tilde{x}}\,d\tilde{x} + \frac{\partial \tilde{h}}{\partial \tilde{t}}\,d\tilde{t}$$

$$= \frac{\partial \tilde{h}}{\partial \tilde{x}}\,(dx - u_o\,dt) + \frac{\partial \tilde{h}}{\partial \tilde{t}}\,dt$$

Hence

$$\frac{\partial h}{\partial x} = \frac{\partial \tilde{h}}{\partial \tilde{x}} \quad \text{is invariant}$$

$$\frac{\partial h}{\partial t} = \frac{\partial \tilde{h}}{\partial \tilde{t}} - u_o\,\frac{\partial \tilde{h}}{\partial \tilde{x}} \quad \text{is not invariant}$$

Similar expansions will show the quantity u_x is invariant, while u_t is not. The constrained flow equations may be expanded in similar fashion and found to be invariant; that is, valid in any reference frame moving at constant speed.

A COMPARISON OF THEORY AND EXPERIMENTS FOR RUN-UP OF SOLITARY WAVES

The objective of developing mathematical methods for the calculation of run-up flows is to provide a more powerful and flexible tool than scale model experiments for studying real problems. Since most models, including the one discussed here by Heitner (2), are approximate, they should be checked against experimental data to determine if they are accurate.

In this case, the experimental data used is that of Camfield and Street (1) for the run-up of solitary waves. Single solitary waves are generated in a tank of rectangular cross section and constant depth by an appropriate motion of piston wavemaker at one end of the tank. The wave propagates down the tank to a portion with a linear sloping beach, where the wave deforms and breaks. This action is recorded by continuously measuring the water surface height at fixed points along the beach with electrical gauges. Typical profiles of the wave deformation process, for two cases of solitary wave run-up are presented. Street (4) has also provided additional data to complete the description of the experiments, so that an accurate comparison is possible.

The run-up calculations are based on the constrained flow model where the horizontal fluid velocity is constant with respect to depth. The equations for this model are solved on a digital computer. For these problems, the computer is programmed to reproduce the geometry of the experimental setup, and generate waves of the correct scale size for the problem. See Appendix F for the generator motion.

A constant coefficient artificial viscosity term of the form

$$a^2h^3(u_x)^2 \, \mathrm{Hysd}(-u_x)$$

is used to allow for the formation of hydraulic shocks in the flow. Here h is the fluid depth, u is the horizontal fluid velocity, and x is the horizontal

coordinate. The function Hysd(x) is given by

$$\mathrm{Hysd}(x) \qquad \begin{Bmatrix} 0 & x \leq 0 \\ 1 & x > 0 \end{Bmatrix}$$

Here $a^2 = 0.3$ is used as a compromise between the excessive attenuation of waveforms where no attenuation is desired and the formation of shocks with large downstream oscillations. The bottom friction is set equal to zero.

The computer solves the equations of the flow model, simulating the experiment. The water surface heights at the wave gauge locations are stored in the computer and obtained as plots on the same scale as the data presented by Camfield and Street.

Two examples are given, summarized by Figures 1 and 2, showing the layout, the experimental results, and the calculated results for each case. The records of η, the wave height above still water, are plotted vs. time, for each of the five wave height gauges. In general, the agreement is reasonably good. It is difficult to determine the sources of error. The constrained flow itself introduces some error, in that it does not permit true fluid motion. This shows up in the fact that the calculated disturbance propagates slightly faster than the experimental results indicate. The solitary wave in the constrained flow model also travels somewhat faster than in the more complete higher order theory of Laitone (3). In addition, the artificial viscosity term tends to round off or attenuate sharper peaks (higher frequencies) in the wave profile. Finally, the original experimental data was on a quite small scale and errors could have been introduced in making the final plots.

Camfield and Street also give data on the run-up of solitary waves on a vertical wall. This case is easily simulated on the computer. Since no shocks are expected to form, the coefficient of the artificial viscosity term

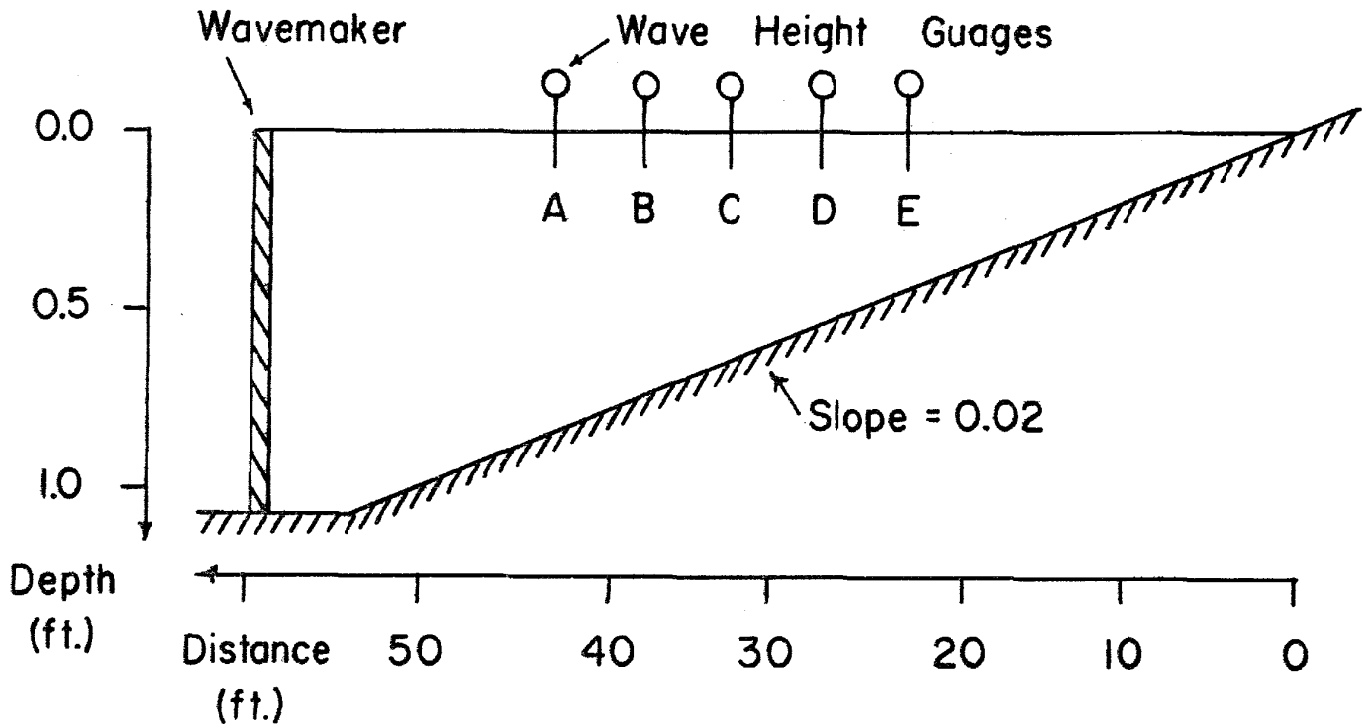

Figure 1(a) - Layout for slope = 0.02 (scale distorted).

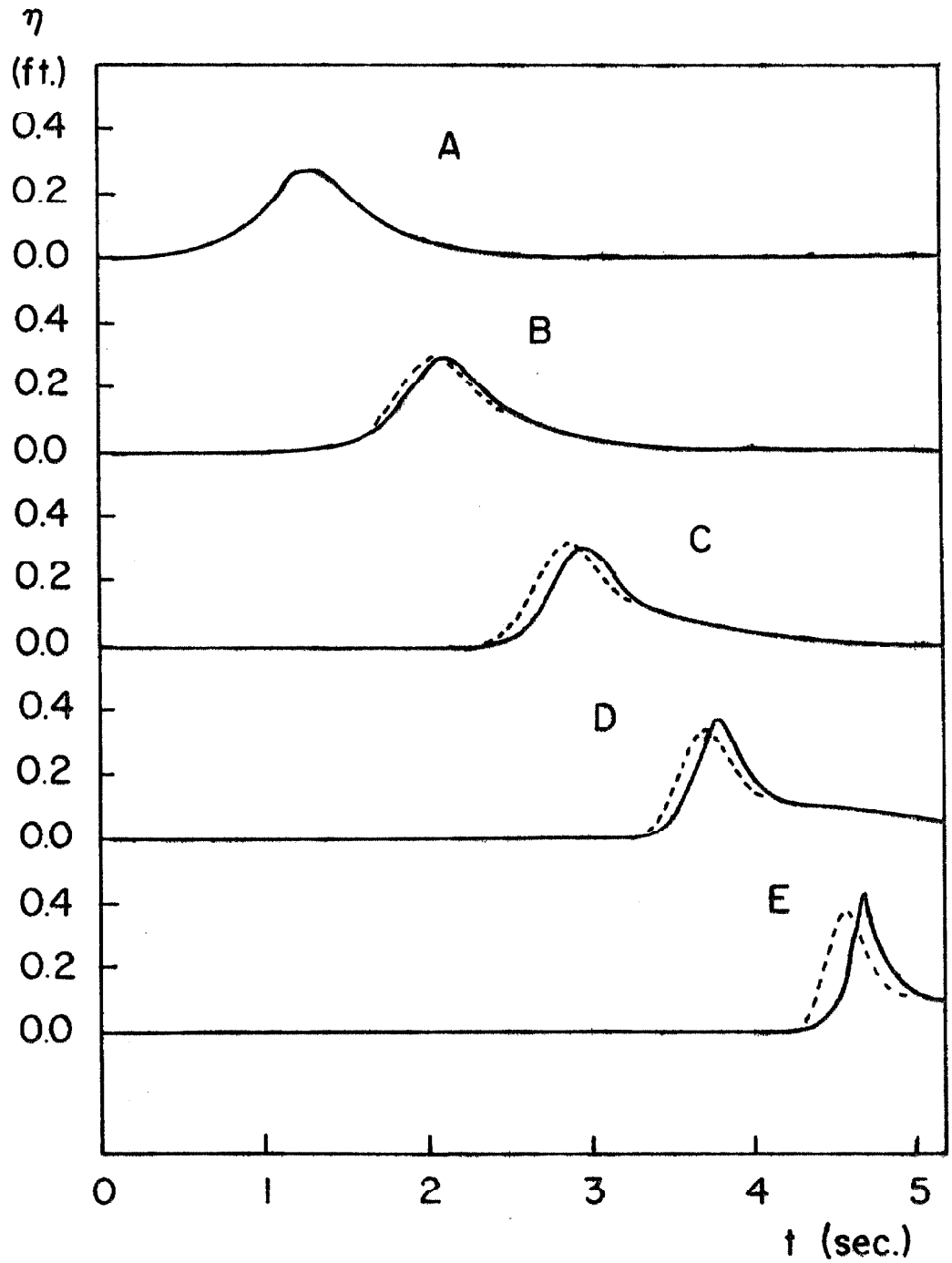

Figure 1(b) - Experimental results for slope = 0.02
(Same as page 86 in Ref. (1)).
Dotted lines are from Figure 1(c).

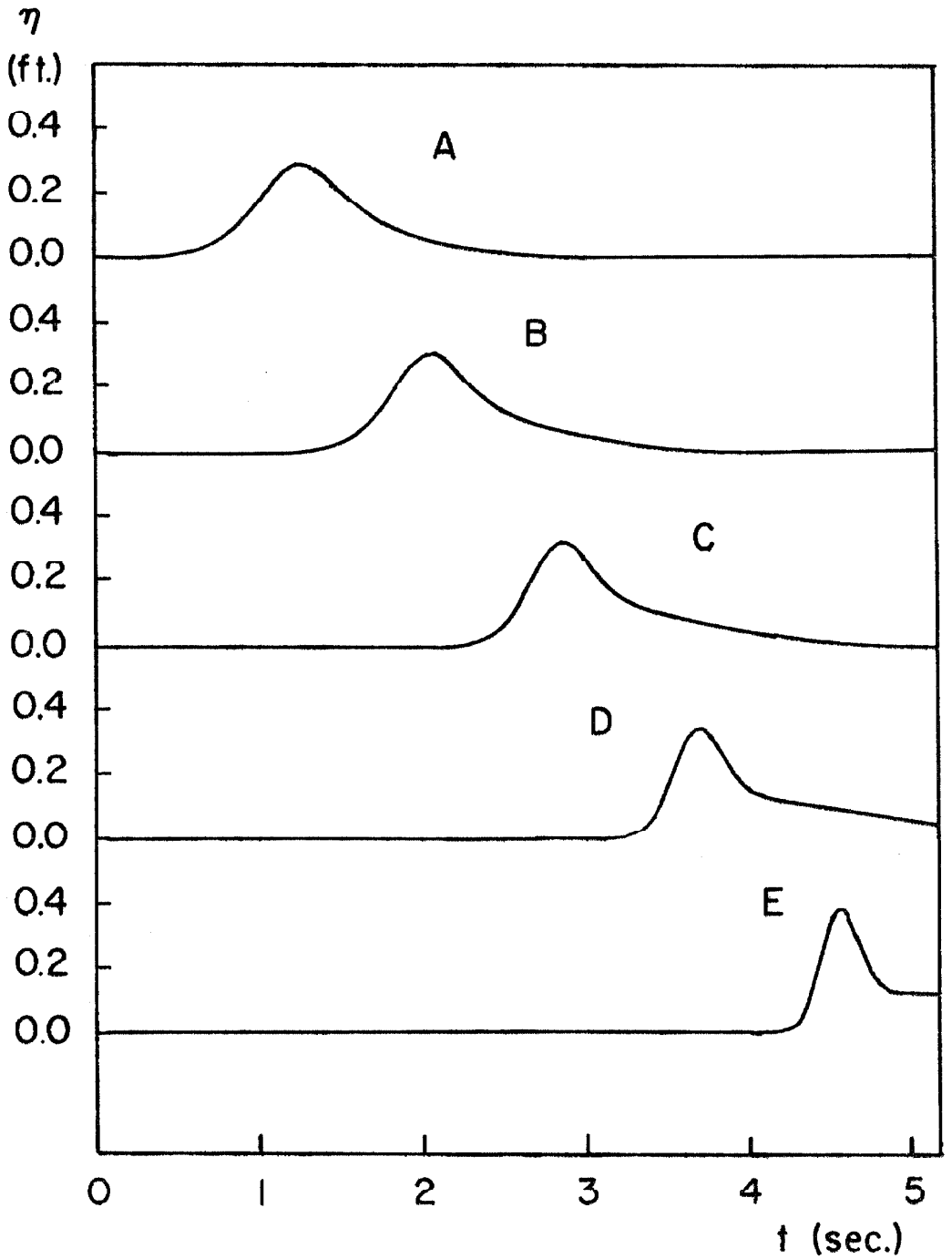

Figure 1(c) - Calculated results for slope = 0.02.

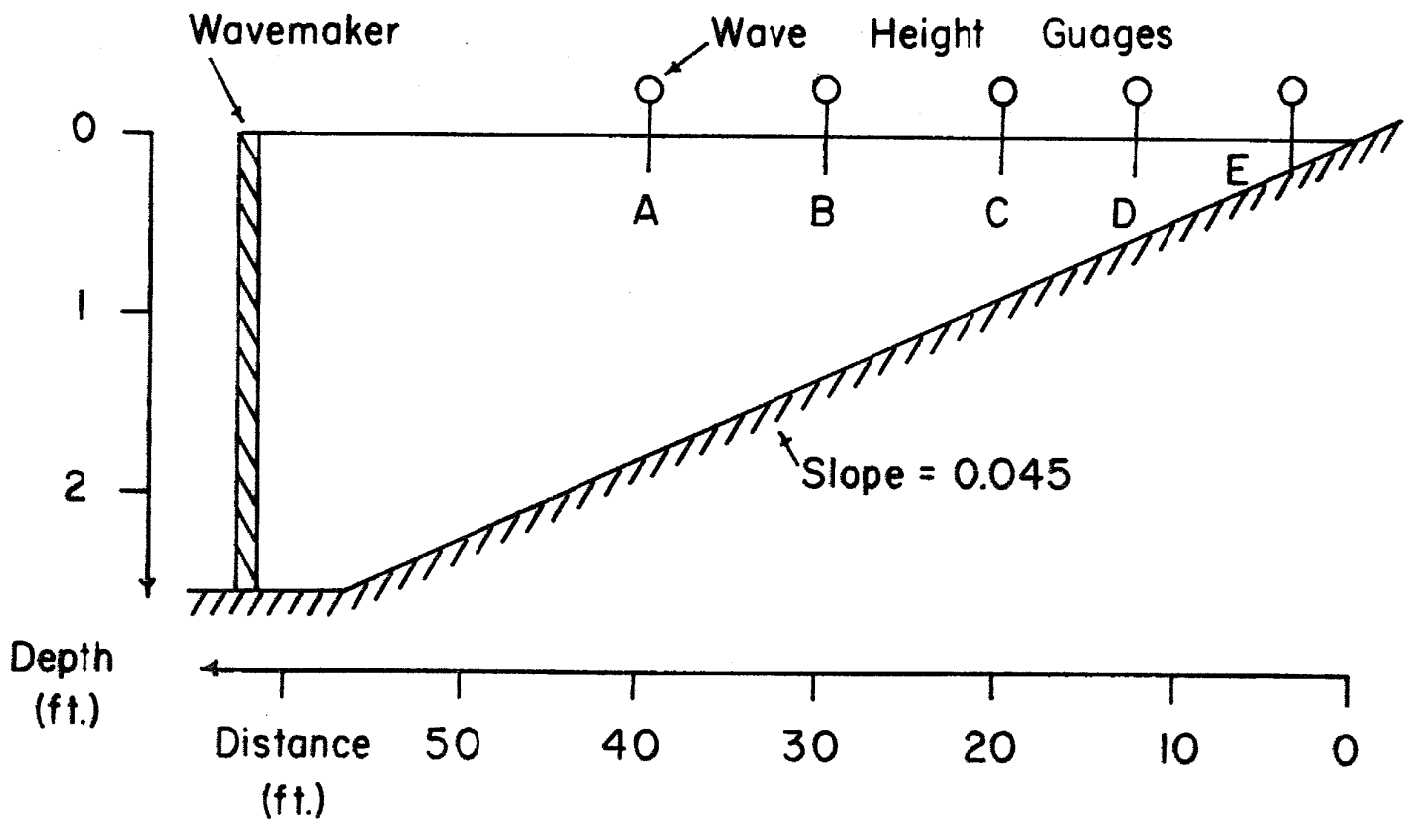

Figure 2(a) - Layout for slope = 0.045 (scale distorted).

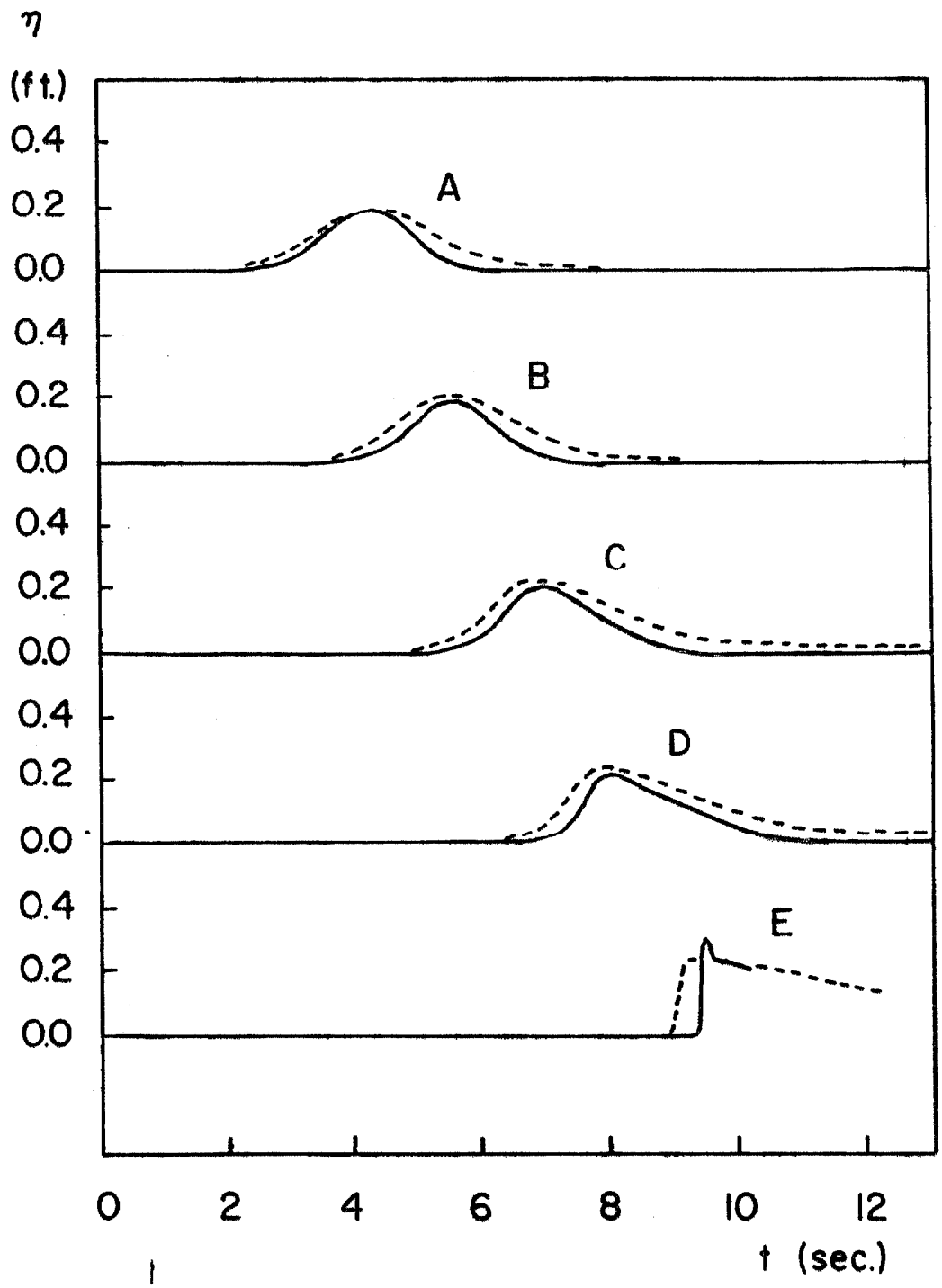

Figure 2(b) - Experimental results for slope = 0.045
(Same as page 88 Reference (1)).
Dotted lines are from Figure 2(c).

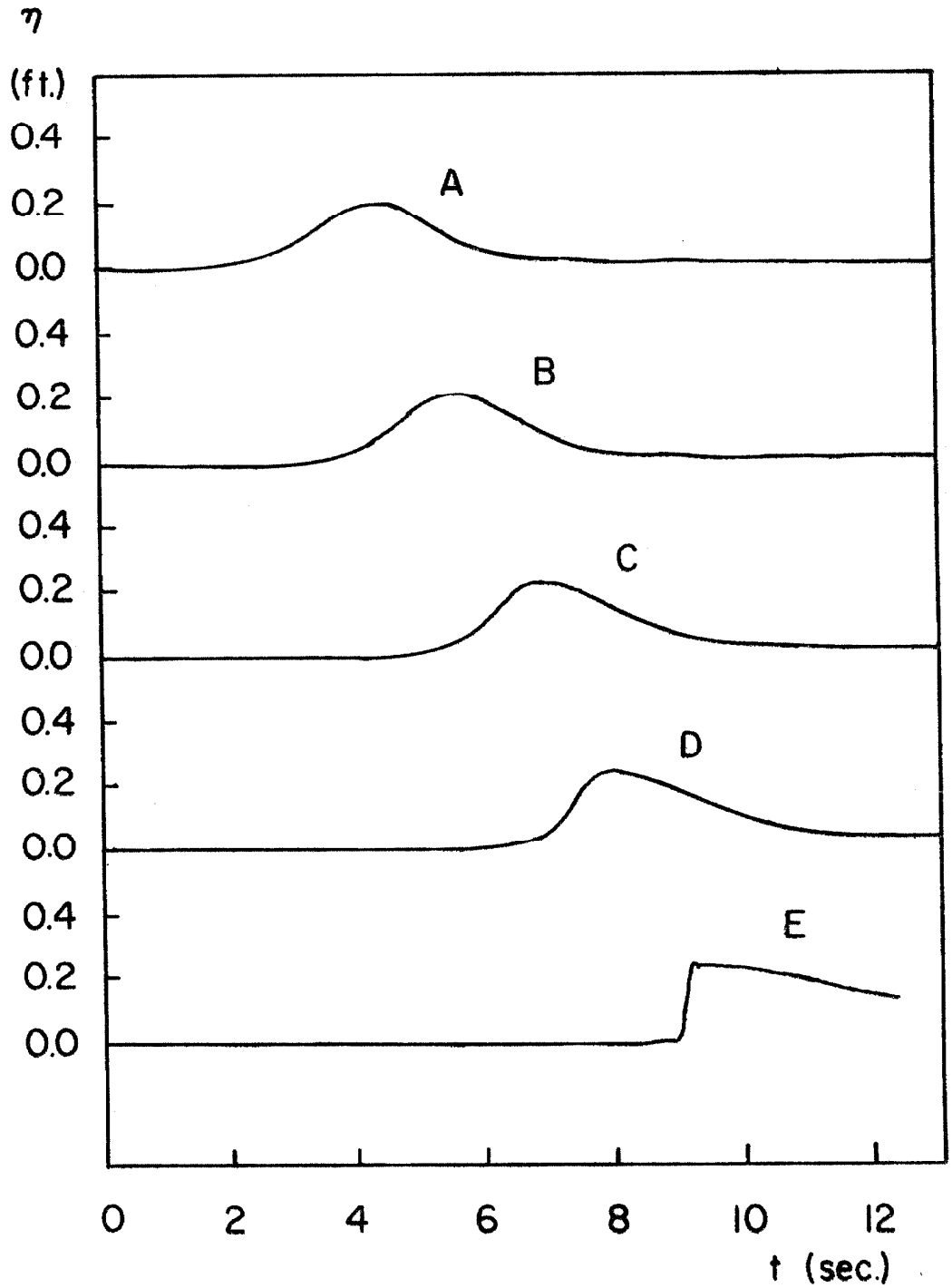

Figure 2(c) - Calculated results for slope = 0.045.

is set equal to zero.

The results are summarized in Figure 3, where D is the depth, H is the wave height above the normal free surface level, and R is the run-up above the normal free surface level. The experiments fall below the calculations for low H/D. This seems to be due to experimental error, since the calculated results extrapolate back to $R/H \rightarrow 2$ for $H/D \rightarrow 0$, which is the result for small amplitude theory and seems to be a reasonable lower limit. For larger H/D, it is not unreasonable that the experimental results would tend to lie above the calculations, because of the limitation of the constrained flow model.

In conclusion, the present comparison of data and calculation show the model is very useful. Even if there is some small error in reproducing the details of the flow pattern, this should not affect the model's usefulness. The important physical variables, such as horizontal momentum (which determines the dynamic forces exerted by the fluid) are preserved very accurately because their conservation is the basis of the governing equations. Slight differences in the distribution of the horizontal momentum will occur, but the total horizontal momentum is conserved. Thus, there is no need to use a two space-dimension model for the flow, unless the detailed distribution of the momentum is important. Of course, such a model would require more extensive computation and more computing time.

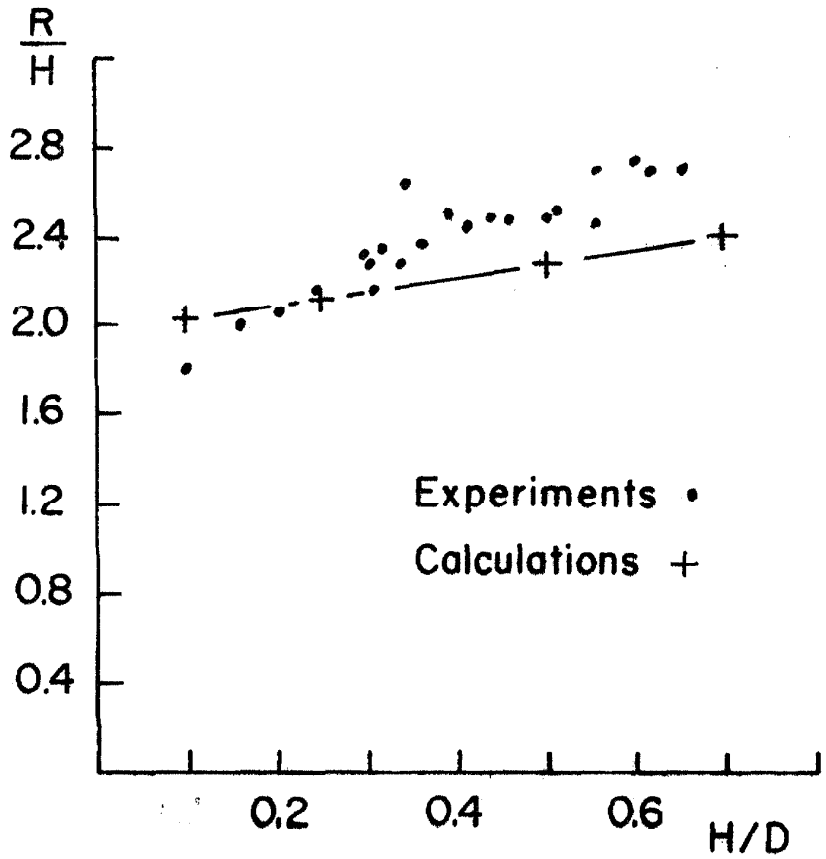

Figure 3 - Comparison of experiments and calculations for run-up of solitary wave on a vertical wall.

REFERENCES

(1) Camfield, F. E., and Street, R. L., On Investigation of the Deformation and Breaking of Solitary Waves, Technical Report No. 87, Dept. of Civil Engineering, Stanford U., Dec. 1967.

(2) Heitner, K. L., "A Mathematical Model for the Calculation of the Run-Up of Tsunamis," Thesis presented to the California Institute of Technology at Pasadena, California in 1969, in partial fulfillment of the requirements for the degree of Doctor of Philosophy.

(3) Laitone, E. V., "The Second Approximation to Cnoidal and Solitary Waves," Journal of Fluid Mechanics, Vol. 9, Part 3, Nov. 1960, pp. 430-444.

(4) Street, R. L., Personal communications with author.

APPENDIX F

Generation of Solitary Waves

For the constrained flow theory, a solitary wave has an exact solution of the form

$$h = h_o + H \frac{2}{1 + \cosh\left(k(x-u_o t)\right)} \tag{A-1}$$

where

$$k = \frac{1}{h_o}\sqrt{\frac{3H}{H + h_o}} \tag{A-2}$$

and

$$u_o = \sqrt{g(h_o + H)} \tag{A-3}$$

Here h is the wave profile height above the bottom, h_o is the still water depth, H the solitary wave height above still water, and u_o the wave speed. (See reference (2)). The wave is considered moving in the positive x-direction. The corresponding horizontal velocity u for this wave motion may be shown to be

$$u = \frac{2Hu_o}{2H+h_o\left(1+\cosh k(x-u_o t)\right)} \tag{A-4}$$

What is needed is to define the motion of the piston wavemaker to produce this motion very accurately. This is done by having the wavemaker acceleration d^2x/dt^2 given by

$$\frac{d^2x}{dt^2} = \frac{du}{dt} = \frac{\partial u}{\partial t} + u\frac{\partial u}{\partial x} \tag{A-5}$$

where (A-4) is used to evaluate the right-hand side of (A-5).

It should be noted that x, the wavemaker position, appears explicitly on the right-hand side of (A-5), and so the wavemaker motion is actually a solution of this ordinary differential equation. However, the numerical integration of this equation can be combined with the integration of the system

representing the fluid mechanics of the problem.

Since the solitary wave form is infinite in extent, the generation time is also infinite. However, a quite accurate truncated waveform is generated by simply setting the right-hand side of (A-5) equal to zero for values of $k(x-u_o t)$ outside of the range $-7.5 < k(x-u_o t) < 7.5$. This will give about a one percent error in the generated wave, which is very difficult to detect visually in the wave profile.